Performance of reinforcements in wood in relation to the service profile

Leistungsfähigkeit von Verstärkungen in Holz unter dem Aspekt des Nutzprofils

Research report

Authors	Steffen Franke Bettina Franke Marcus Schiere
Project Leader	Prof. Dr. Steffen Franke
Head of the Institute	a. I. Martin Geiser

Bern University of Applied Sciences
Institute for Timber Constructions, Structures and Architecture

Zusammenfassung

Holz ist ein leistungsfähiges natürliches Konstruktionsmaterial. Zur Verbesserung der Eigenschaften in Fügepunkten oder hochleistungsfähigen gebogenen und gekrümmten Trägern kommen mechanische Verstärkungen zur Anwendung. Die generelle Bemessung der Tragfähigkeit dieser eingesetzten Verstärkungen ist bekannt. Aber wie wirken sich feuchteinduzierte Spannungen im Holzquerschnitt auf die Verstärkungen aus?

Die mechanischen und physikalischen Eigenschaften von Holz sind abhängig vom Feuchtegehalt des Holzes. Da Holz ein kapillar poröses Material ist, ist es in der Lage aus dem Umgebungsklima Wasser aufzunehmen respektive abzugeben. Eine Änderung des Holzfeuchtegehalt beginnt immer an der Oberfläche und führt zu einem Feuchtegradienten über den Querschnitt des Tragelementes. Die Änderung des Feuchtegehaltes führt zum Schwinden respektive Quellen des Holzes. Diese Verformungen können sich aufgrund des Feuchtegradienten nicht frei ausbilden und führen zu feuchtinduzierten Spannungen (MIS moisture induced stresses) im Querschnitt. Die MIS werden durch mechanische Verstärkungen und Anschlüsse zusätzlich beeinflusst.

Die Forschungsarbeit versucht in experimentellen Untersuchungen diesen Effekt zu bewerten und dem planenden Ingenieur Empfehlungen für die Bemessung zu geben. Aktuell sind hierzu keine Angaben in den europäischen und nationalen Standards enthalten. In den Prüfserien sind Brettschichtholzquerschnitte in den Höhen 600 mm und 1000 mm betrachtet wurden. Als Verstärkung sind Gewindestangen mit einem Durchmesser von M16 eingedreht. Die Stirnseiten wurden unversiegelt für den Effekt eines Endträgers und versiegelt für die Bewertung des Effekts in Mitte der Trägerlängsachse ausgebildet. Insgesamt verteilten sich 28 Prüfkörper auf 9 Varianten und drei verschiedene Klimaszenarien zum Abtrocknungsverhalten. Das Umgebungsklima in Holztragwerken unterscheidet sich durch das Nutzungsprofil (z.B. Reithalle, Sporthalle oder Eisstadien) oder verändert sich durch die Phasen der Errichtung und Inbetriebnahme. Die zu erwartende Holzfeuchtegehalte sind aus Veröffentlichungen abgeleitet worden.

Für die Bewertung des Trag- und Verformungsverhaltens wurde die Entwicklung der Holzfeuchtegehaltes über die Zeit und den Querschnitt erfasst. Zu definierten Zeitpunkten wurden die Verformungen des gesamten Prüfkörpers in Trägerhöhe wie auch die der Verstärkungen gemessen. An repräsentativen Prüfkörpern wurden zusätzlich Verstärkungen mit innenliegend applizierten Dehnungsmessstreifen verwendet. Im Ergebnis konnten anhand der erreichten Messwerte, unter Anwendung von analytischen Berechnungsverfahren für nachgiebig zusammengesetzte Querschnitte, spezifische Quell- und Schwindmasse sowie Beanspruchungen der Verstärkungen von verstärkten Brettschichtholzträgern abgeleitet werden.

Zusätzlich zur bekannten Traglastanalyse kann der Ingenieur hiermit eine Abschätzung der Wirkungsweise von Verstärkungen unter klimatischer Beanspruchung vornehmen. Hierfür sind Grafiken und Berechnungsbeispiele erarbeitet worden. Der Zeitpunkt der Implementierung der Verstärkung, wie u. a. während der Produktion oder innerhalb der Errichtung, ist auch für das Trag- und Verformungsverhalten zu beachten.

Keywords: Feuchteinduzierte Spannungen, Verstärkungen, Schrauben, Holzbauteile

Abstract

Wood is a high-performance natural material. Mechanical reinforcements are used to improve the properties of joints or high performance curved and bent beams. The general design of these reinforcements is well known. But how do moisture-induced stresses in the timber cross-section affect the reinforcements?

The mechanical and physical properties of wood depend on its moisture content. As wood is a capillary porous material, it can absorb and release water from the surrounding environment. A change in the moisture content of wood always starts at the surface and results in a moisture gradient across the cross-section of the structural member. The change in moisture content causes the wood to shrink or swell. These deformations cannot form freely due to the moisture gradient and result in moisture induced stresses (MIS) in the cross-section. MIS are also influenced by mechanical reinforcements and connections.

The research will attempt to evaluate this effect in experimental studies and provide design recommendations to the designer. At present there is no information on this in the European and national standards. In the test series, glulam cross-sections with heights of 600 mm and 1000 mm were considered. Threaded rods of M16 diameter were screwed in as reinforcement. The end faces were unsealed to evaluate the effect of an end beam and sealed to evaluate the effect at the centre of the longitudinal beam axis. A total of 28 specimens were tested in 9 variants and three different climatic scenarios for drying behaviour. Ambient climates in timber structures vary according to the use profile (e.g., indoor riding arena, sports hall or ice stadium) or changes due to the construction and commissioning phases. The expected wood moisture contents are derived from publications.

To evaluate the load-bearing and deformation behaviour, the moisture content of the wood was recorded over time and across the cross section. Deformations of the whole specimen were measured at beam height and in the reinforcement at defined times. In addition, reinforcements with internal strain gauges were used on representative specimens. As a result, specific swelling and shrinkage masses for the climate-induced expansion behaviour of reinforced glulam beams could be derived from the measured values.

In addition to the known ultimate load analysis, the engineer can use this to estimate the effect of reinforcement under climatic stress. Graphics and calculation examples have been developed for this purpose. The time at which the reinforcement is applied, e.g., during manufacture or erection, must also be taken into account for the load-bearing and deformation behaviour.

Keywords: Moisture content, moisture gradient, moisture induced stresses, monitoring campaigns, quality assurance, moisture content simulation, building environments

Acknowledgements

Table of Content

1 Introduction

1.1 Influence of service profiles on reinforcements in timber structures

The counterpart of reinforcements or prestressed steel bars in concrete construction are fully threaded screws or threaded rods in timber construction. Reinforcement of connections or timber members becomes necessary when the architect restricts cross-sectional geometry or if curved, notched, and perforated members are used. However, the advantages of reinforcement measures, such as the increase in load-bearing capacity and ductility, are also confronted with many complex issues.

Especially for internal invisible mechanical reinforcements, there is a lack of knowledge about the real stresses in the fasteners. In addition, reinforcements change/restrict the free deformation behaviour of the cross-section due to shrinkage and swelling and result in additional moisture-induced stresses which may cause deep cracks to appear on the surface during drying. These cracks influence not only the aesthetics but also the overall load-bearing capacity of the structure.

Published research on internal reinforcements was mainly done in constant climate. There are first experiences available for reinforced beams under varying dynamic climate, although varying climatic stresses occur not only in exterior components but also in interior components in non-air-conditioned structures or through specific user profiles. Designing engineers of fully threaded screws and screwed-in threaded rods are aware of the lack of knowledge and asking for assistance from research institutions.

The objective is to provide answers to the load-bearing behaviour of reinforced timber constructions for both the planning timber engineer and the manufacturer in the research application. The focus is on systematically defined experimental investigations on glulam beams of practical relevance. The results form the basis for an empirical model for practical use and the validation of the accompanying numerical model. Realistic climate situations were tested in climatic chambers to evaluate the load-bearing capacity of reinforcements. The measurement results obtained were used to eliminate uncertainties for timber construction engineers and reduce damage in a wide range of applications. The research results promote the use of wood by ensuring quality, performance, and aesthetics in timber constructions.

1.2 Goal and objectives of the project

The objective of the research project is to evaluate the load-bearing capacity of internal mechanical reinforcements under varying climate conditions. The focus is on self-drilling fully threaded screws and threaded rods, which are arranged in one or more rows across the cross-sectional width. The variation of the parameters takes place in the bearing cross section and the considered climatic stresses and reinforcement measures. For the evaluation of the interaction between static load-bearing capacity and dynamic climatic stress, experimental investigations are planned with the following focal points.

- ▸ Systematic variation of reinforcement (single row, double row, reinforcement near end grain), cross-section geometry and relevant climates
- ▸ Development of an empirical model for practice to evaluate the most important parameters based on the experimental results.
- ▸ Discussion of the results and recommendations to be derived with the manufacturers and engineers from the field at regular intervals.

In the research application, the outcomes were defined as follows:

- ▸ Overview of materials, reinforcements, and climates with evaluation as safe/unsafe,
- ▸ Test program to evaluate the interaction of transverse tensile reinforcements with the required climatic stress for experimental and numerical implementation,
- ▸ Empirical model as well as hints for use in practice.

The results thus improve the understanding of reinforcements. High-risk applications can be avoided or better dimensioned. Better measures can also be derived in existing situations, thus increasing the recognition of wood as a quality-assured construction material in society and at the same time increasing wood sales in Switzerland.

1.3 State of Art

1.3.1 Reinforcement in timber structures

Reinforcements in timber structures have opened new perspectives through the development and use of self-drilling fully threaded screws and threaded rods as shown, among others, in Blaß et al. (2006, 2010, 2017), Dietsch (2012, 2017), Lauber (2008), Trautz (2017), Trautz & Koj (2008). The statical short term load bearing behaviour of reinforced beams with holes were investigated by e.g., Danielson (2013) and beams with unreinforced and reinforced notches by e.g., Jockwer (2014). The tests by both researchers were carried out in constant ambient climates. Jockwer states that one argument for reinforcing notches is to reduce damaging moisture effects. In Steiger et al. (2015), there is an evaluation/overview of the application of threaded rods glued-in as reinforcement measures. Data on the application of screwed-in threaded rods or fully threaded screws are hardly given. Compared to glued-in threaded rods (Steiger et al. 2015), self-drilling full-thread screws represent an economically better reinforcement measure. Threaded rods with a diameter of 20 mm have larger diameters for higher load-bearing capacities than fully threaded screws with 14 mm.

For the design of reinforcements in timber structures, SIA 265:2012 provides information in Annex D for the reinforcement of transverse connections, notches, openings, and pitched roof beams. In addition to the calculation of the design value of the tensile force acting on the reinforcement, structural information is given on the distances between each other and from the edge of the notch and opening and the insertion length for curved or pitched roof beams. Guidance on the consideration of additional moisture-induced stresses due to single or varying climate changes is not given in SIA 265:2012, nor in SN EN 1995-1-1-:2004. A design proposal for the consideration of moisture-induced stresses of threaded rods glued into the wood is given in the publication by Gerold (1992) and Ehlbeck et al. (1992). This is used as a starting point for screwed-in threaded rods or fully threaded screws in the research project.

Internal screwed reinforcements in glulam beams are used in (Figure 1 and Figure 2):

- ▸ Cambered beams
- ▸ Curved beams
- ▸ Tensile reinforcement around secondary load bearing members.
- ▸ Notches and holes in beams
- ▸ Reinforcement for compression in supports.
- ▸ Shear reinforcement around highly loaded supports.

1.3.2 Reinforcements under varying climate loads

Reinforcements in the form of fully threaded screws or screwed/glued-in threaded rods restrain the free shrinkage and swelling of wood. The fact that damage can occur even in reinforced curved and pitched roof beams, support areas, notches and holes is well known, i.e., Dietsch & Brandner (2015), Franke et al. (2015), compare Figure 3. For non-visible internal reinforcements, moisture-induced stresses should be considered in these special cases, as the reinforcements are located close to the timber surface, see Dietsch & Brandner (2015) or further in Gustafsson et al. (1998). In these areas, a very quick change in wood moisture content occurs as the ambient climate changes. However, how this can be considered in practical design methods has not yet been indicated. The following research work provides initial findings and indicates the need for further research to develop a practice-relevant model for estimating the load-bearing capacity.
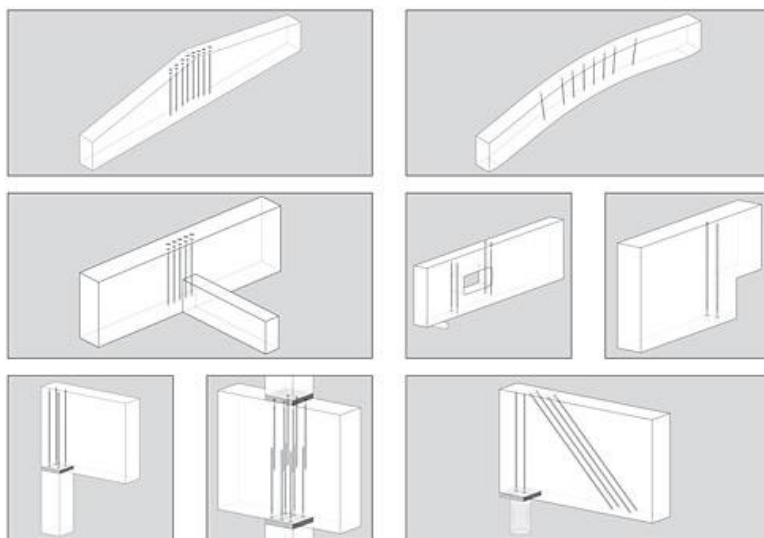
Figure 1: Principal sketches of transverse tension reinforcements, transverse compression reinforcements and shear reinforcements in timber construction, www.SFS-intec.biz (12.09.2018)

Figure 2: Transverse tensile failure of a pitched roof girder (top), production of curved beams with reinforcements by threaded rods (bottom), Brüninghoff (2007)

Figure 3: Cracked unreinforced glulam beams (top) free shrinkage with smaller cracks (top left), deep shrinkage cracks between fasteners (top right) and cracks in reinforced glulam beams (bottom), Dietsch (2017)

Figure 4: Reinforced glulam test specimens after 90 days of climate drying load, test specimen length of 320 mm, test specimen height of up to 1280 mm, Wallner (2012).

Angst & Malo (2012) show in test results and numerical simulations that different glulam constructions and dimensions strongly influence the load-bearing behaviour and that the steel strength are sometimes reached and even exceeded. Furthermore, it is pointed out that self-drilling fully threaded screws as reinforcement negatively influence the material behaviour of timber in drying situations. Koj & Trautz (2014) carried out long-term tests on moment rigid frame corners in an outdoor climate. Here, only the reduction of the overall load-bearing capacity was tested, a detailed measurement and evaluation of the different load-bearing behaviour of reinforcement itself was not given.

The work by Dietsch (2017) also provides initial test and simulation results on the effect of reinforcements under shrinkage stresses. Using drilled-in threaded rods with Ø 16 mm in glulam beams of 200 mm/1000 mm, it could be proven that cracks develop from stresses of 0.54 N/mm². The stress level is equivalent to a moisture change of 1.3 M%. However, the test results were carried out on cyclic short-term tests, which means that long-term effects/relaxations are neglected. Relaxations of 50 % are realistic according

to SIA 265/1 and Aicher & Dill-Langer (1997) and would theoretically double the determined moisture change. Dietsch (2017) also states that a moisture reduction of 1 % already cancels out the effect of the reinforcement measure. This was calculated for a curved beam and 50 % relaxation. A further moisture reduction of 1 % already results in transverse tensile stresses of approx. 0.5 N/mm^2.

Wallner (2012) investigated glulam beams (160/1280 mm, in the lengths 160, 320, 640, 1280 mm) which were first conditioned at 90% relative humidity for 18 months, then reinforced with fully threaded screws and exposed to a constant ambient climate with 40% relative humidity. The load-bearing behaviour of the screws and the wood was measured continuously. Figure 4 shows the test specimens after 90 days of climatic load, the severe cracking and deformation. Wallner (2012) only investigated processes during restricted shrinkage. There are no studies on restricted swelling, where tensile stresses in the screw can overlap with tensile stresses from external loads, and under varying climates. Likewise, the increasing influence of end-grain moisture transport was not considered.

1.3.3 Measuring methods for stresses in reinforcements

Dietsch (2017) and Trautz (2017) used a photogrammetric method, such as Digital Image Correlation (DIC), to record the strain and deformation behaviour of glulam with screws under load. This makes it possible to visualize the interaction between the screw and the wood on the surface. This method can be used in static short-term tests under constant ambient climate. This measuring method is not suitable for long-term tests and under varying climatic stresses, which can only be carried out in a controlled manner in climatic chambers.

A second measuring method is the use of strain gauges. On the one hand, strain gauges were glued into a cavity inside the fastener, Dröscher (2016), Figure 5, or on the other hand outside in a special area with a reduced cross-section, see Wallner (2012), Figure 6. Both measuring methods are innovative but weaken the fastener or sometimes influence the load bearing and failure behaviour of the wood as can be seen in the failure pictures by Wallner (2012).

For recording the forces in the fastener without weaken the fastener itself, the use of miniature ring load cells as shown in Figure 7 could be an option. In the experimental studies by Wallner (2012), forces of up to 88 kN were measured within one year in non-cracked beams. On average, the forces concentrate at approx. 20 kN within the test program. These forces can be measured reliably over a longer period using ring load cells or load sensors. This measurement method has not been discussed in literature sources so far and could be evaluated by combining it with the previous measurement methods.

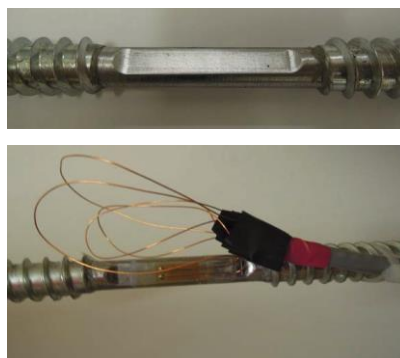*Figure 5: Strain gauges inside the reinforcement, source: Dröscher (2016)*

Figure 6: Application of strain gauges on reinforcement, source: Wallner (2012)

Figure 7: Ring load cell, source: product catalogue Burster Präzisionsmesstechnik (2016)

2 Basic principles for the research project

In work package 1, the aim is to define the relevant materials, mechanical reinforcements, and cross-section sizes together with the project partners in a workshop. Furthermore, the relevant climate scenarios regarding drying, wetting, changing climates and possible extreme situations needed to be defined. As a result, the test program with the climatic load is defined. The climatic loads are derived from a data base. The cross-section sizes in the test program result from the information provided by the practice partners and the standards.

2.1 Material and reinforcement techniques

Glulam that is produced from softwood like spruce is still one of the most important building materials in modern timber construction industry. Glulam products with hardwoods like beech, oak, and ash are used more and more frequently. However, more truss-like structures or beams with smaller spans are built with these materials, unlike the large beams or block glulam beams seen with the softwood species. This is still due to higher costs related to the use of hardwoods in timber structures.

Focus of research projects with reinforcement of timber is until now primarily carried out with softwood timber (Blass 2010, Dietsch et al 2018, Danielsson 2014, Danzer et al. 2020). The sounding board committee of this project judges that the work that was to be carried should be focused on softwood.

Widths of glulam beams in modern timber engineering range between 160 mm and 240 mm (Figure 8) (Gamper et al., 2014). These can also be glued together sideways to form block glulam beams (Franke et al. 2019). Block glulam beams in buildings are up to two single beams wide. In bridges, these can be over 1.6 m wide like in the Horen Bridge in Küttingen (CH). In discussions with practicing engineers, the heights of glulam beams range from 600 mm to 2000 mm and rarely over 2000 mm. The maximum heights of glulam beams for the project were, therefore, set to 2000 mm.

Reinforcements are used to improve the shear and perpendicular to grain tensile load-bearing capacity. By adding stiff components to weaker material, developed (internal residual or externally applied force) stresses avert the weak material.
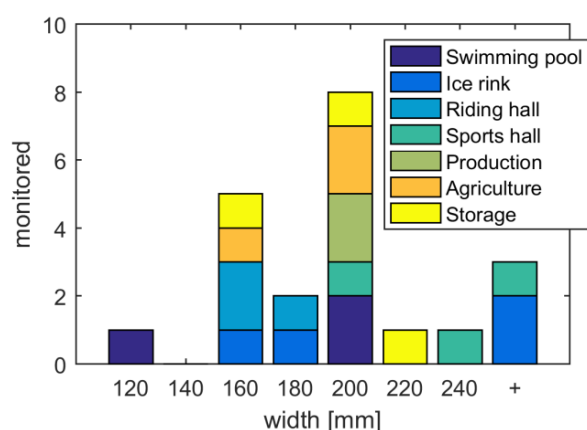

Figure 8: Cross-section dimensions from 21 buildings monitored in southern Germany (Gamper et al. 2014)

Figure 9: The monitored Horen bridge close to Aarau that crosses a road, photographed from the north side. The width of the load-bearing beams is about 1600 mm.

Factors constraining swelling and shrinkage in varying climates are (based on a list published in Jockwer (2014):

- ▸ Internal reinforcement
    - Glued-in rods
    - Threaded rods or screws

- ▸ External reinforcement
    - Punched nail-plates
    - Adhered wood bases panels

- ▸ Connection to other structural members
    - Slotted-in plates
    - Limited by contact to other structural components

- ▸ Differences in stiffness throughout the material
    - Difference between radial and tangential stiffness
    - Reaction wood (tension or compression)

- ▸ Material inhomogeneity
    - Knots, resin pockets
    - Damaged wood

The first three of the lists are considered as mechanical constraints and are extensively studied in literature and applied in structures. The last two of the lists are inherent to wood material and can only be smoothen by a strong degree of homogenization. All the studies of the development of moisture induced stresses perpendicular to grain could however be assigned to difference between radial and tangential stiffness. Focus lies on internal the reinforcement of glulam through threaded rods or fully threaded screws.

2.2 Climate Scenarios

2.2.1 Annual variations of climates in timber structures

Structural damage related to moisture was quantified by a study in which existing buildings in southern Germany were assessed. Moisture accounted for half of the observed structural damage: too wet, too dry, or varying moisture conditions (Frese and Blass, 2011). The latter accounted for approximately one sixth of the damage in need of repair (Dietsch and Winter, 2018). About 90 % of the encountered damage was found in glued laminated timber. The damage not related to moisture content concerned wrong assumption of loads or errors in calculation of load-bearing capacities for instance.

Climate in a building varies throughout the year. In heated structures (generally SC1), relative humidity in winter is lower than in summer. In buildings that are not heated but ventilated (generally SC2), relative humidity in summer is low whereas this increases towards autumn/winter.

The annual variations were simplified in Franke et al. (2019). Climate was modelled as a sinus that represented the annual variation of relative humidity/equilibrium moisture content (Table 1). In January, moisture contents in ventilated buildings are high and moisture contents in heated buildings are low. These two building climates meet in summer to 12 M%, a value also known as the moisture content during production. The variation of climate can be adjusted according to building type (Figure 10).

A second diagram in Table 1 shows a step climate. This climate represents the climate experienced by the wood in special events such as a building erection or maintenance, which are mainly over a short period of time. Such examples are also given in Franke et al. (2019).

Table 1: Illustration of simplified climate using sinuses or a step shape climate

Model of change of climate according sinuses shape
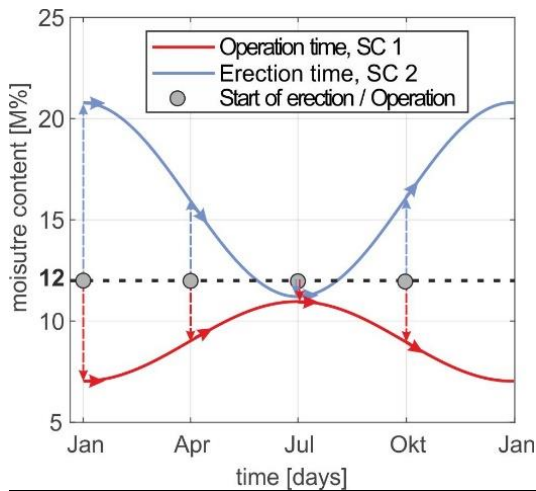
$$u(t)_{SC1} = 9 + \frac{\Delta u_{Surface}}{2} \cos\left(2\pi \frac{t}{365} + \pi\right) \tag{1}$$

$$u(t)_{SC2} = 16 + \frac{\Delta u_{Surface}}{2} \cos\left(2\pi \frac{t}{365}\right) \tag{2}$$

where:

$$\Delta u_{Surface} = \Delta u_{15\,mm} \cdot r_u$$

t Time in Days, $t = 0 \; \hat{=} \; 1^{st}$ of January

(3)

Model of change of climate according step change

$$u(t \le 0) = 12\,\text{M\%}$$
$$u(t > 0) = 12\,\text{M\%} + \Delta u \tag{4}$$

2.2.2 Summary of typical climates in and around timber structures
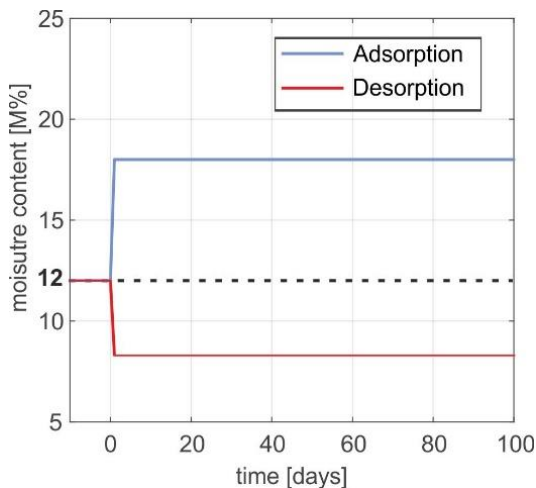
Climates inside and around load bearing elements of timber structures are plotted in Figure 10. The plotted diagrams contain envelopes (minimum and maximum value) of relative humidity and moisture content measured over a minimum of a year in a total of nine different building types. In addition to the curves, the average values, and the deltas at a measuring depth of 15 mm are included. Each box in the diagram represents one monitoring object in Switzerland or Southern Germany (Gamper et al., 2014) and Franke et al, 2019). The following observations concerning these structures are made. These concern the observations in the monitored data and exceptions are possible:

▸ *Swimming pools:* the measured climate contained several blind spots, but graphs with moisture content show stable conditions in general. The climate in the monitored structures was regulated. Measured relative humidity ranges between 40% and 55%. This is in climatised buildings. The moisture content variations throughout the year are stable.

▸ *Sports halls:* Relative humidity and corresponding moisture content are low to very low. Moisture contents might be a little higher than that observed in the production halls. Moisture contents are lowest in winter and increase towards the summertime. Measured relative humidity ranges

between 20% and 65% for three buildings, corresponding moisture contents were between 6 M% and 11 M%. Annual moisture content variations are low.

▸ *Production halls:* Moisture content and climate profiles are like that of the sports halls. Climates might be dryer with relative humidity ranging from 20% to 55% and moisture contents that do not exceed 9 M%. Moisture contents in wintertime are lower than in summertime.

▸ *Ice rinks:* Two ice rinks were heated/climatized, two had a closed building envelope (not heated or climatized) and two were well ventilated. Moisture contents in the climatized ice rinks are generally lower than in the ventilated structures. Relative humidity in climatised buildings can be as low as 40%, but nearly 100% on reference locations in the open and ventilated structures.

▸ *Riding rinks:* Although the structures are closed, large variations in climate are observed. Climate in the building presumably follows the climate around the building to a large extent meaning that moisture contents in winter are higher than in summertime. In summer, relative humidity ranges from 50% to about 95% in winter. Moisture contents subsequently show fluctuations from 12 M% to 18 M%.

▸ *Livestock halls:* The agricultural buildings contain livestock and were often well ventilated through one side of the building being fully open. Yiang et al. (2017) conducted an extensive monitoring campaign in these building types, particularly focused on the risk of wood decay. High moisture load is caused by cleaning (with water) that is required regularly. It is also argued that the evaporation of sweat and breathing of the livestock contributes to the high relative humidity encountered in the structures. Relative humidity ranges from 40 % to 90%. Moisture contents range from 12 M% to 18 M%.

▸ *Storage halls:* The storage halls contained a closed building envelope, but through which smaller doors or windows ventilation was possible. These structures contain the lowest moisture contents of all the ventilated structures. Relative humidity ranges from 45% to 95%. Moisture contents range from 11 M% to 17 M%.

▸ *Skiing stations:* The instrumented ski stations in the alps show moderate moisture content and climate envelopes throughout the year. One of these stations shows high variation in surrounding climate, but as these peaks are only of short duration, they do not lead to high moisture content variation throughout the year. The station is located just behind a mountain ridge between the northern pre-alps and the inner alps. Relative humidity ranges from 30% to 95%. Moisture contents range from 11 M% to 17 M%.

▸ *Timber bridges:* Envelopes of moisture content and climate around the bridges is plot in the last diagram. Moisture content measurements were made in eight bridges, but as some measurements were made deep into the timber material, it was not possible to extrapolate measurements made there to moisture contents at 15 mm depth. This extrapolation is only possible up to depths of 50 mm. The climate in bridges is like that in the reference locations of the ice rinks, i.e., between 50 % and 95 % relative humidity.

Figure 10 also shows that, assuming glulam would be produced between 8 M% and 15 M%, that it would dry for use within heated structures and moisten for use in ventilated structures. Moisture content variations in heated structures are lower than those in ventilated structures.

The lowest moisture content in ventilated structures was observed in the storage halls. Within the heated structures these are seen in the production halls. In the alpine structures, climate was relatively dry and stable throughout the year, varying between 60 %RH and 80 %RH.
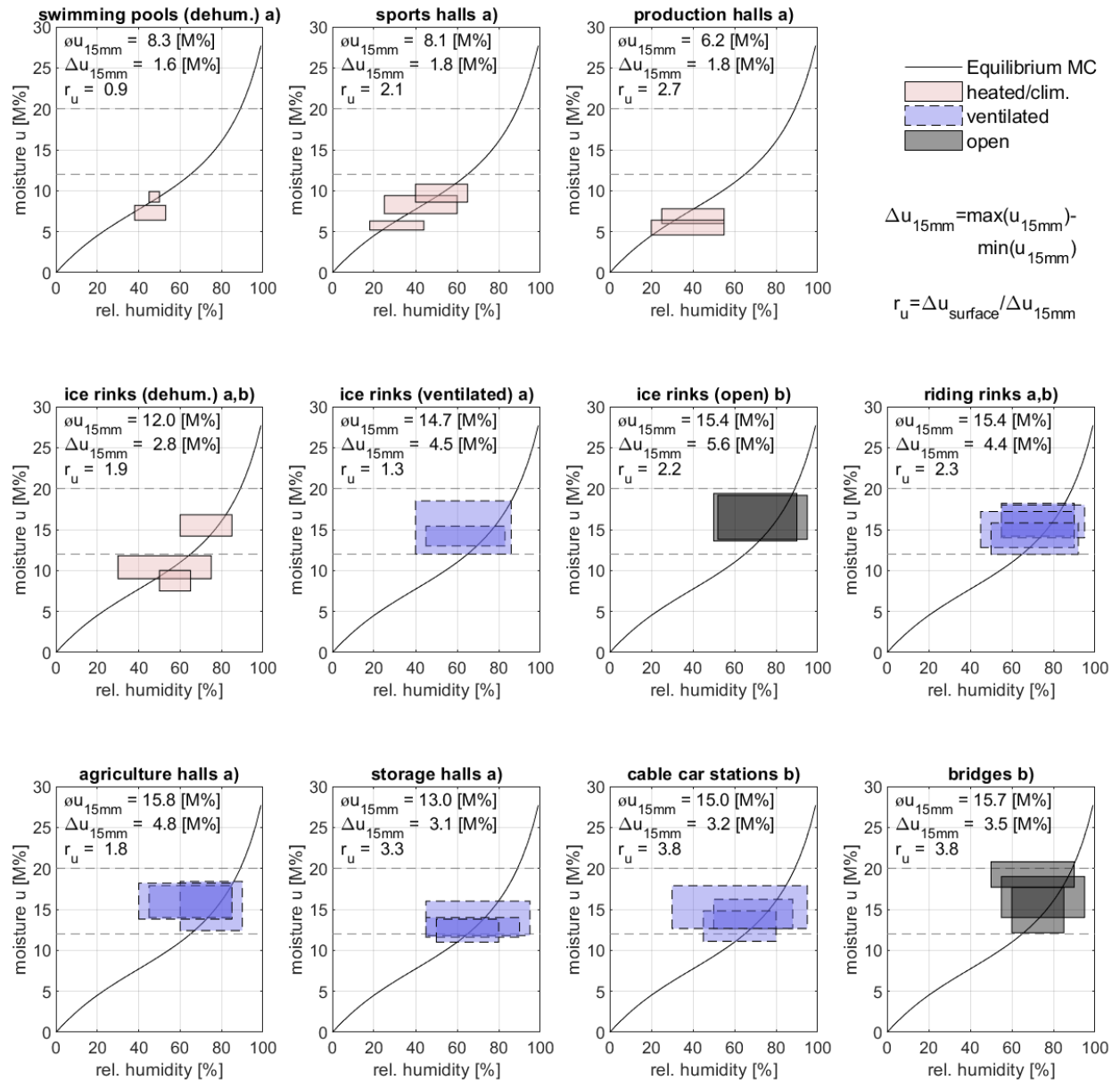
Figure 10: Overview of relation between the envelopes of measured relative humidity and measured moisture content at 15 mm depth from the surface; a) Measuring data based on Gamper et al. (2014) and b) based on Franke et al. (2019)
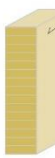
3 Experimental investigations

3.1 Test programme

Based on the aim of the investigations and requirements, the following test programme was chosen. The standard beam width is set to 160 mm, corresponding to the mostly used width in timber structures, compare Figure 8. This also allowed a sufficient moisture diffusion during the climate scenarios and the development of moisture distribution over the width. The timber samples either had a height of 600 or 1000 mm. The element lengths were either 160 or 320 mm, in line with work performed by Wallner (2012). The complete test programme was split into two test series. The first series was performed in Autumn 2019 with 10 elements, the second in Summer 2020 with 18 Elements. The test programme was approved by the expert committee of engineers in the first milestone of the project. The elements were provided by Roth Burgdorf AG. Figure 11 shows an overview of the samples used in both test series and how these were reinforced. The end grain of some elements was not sealed to simulate the moisture impact at open end grain situations like at notches or holes in the elements. The sealed elements were expected to be representative for continuous members. The end grain sealing was performed with aluminium tape. The diameter of the reinforcement was constant 16 mm.

The size of the test specimens was chosen such that the reinforcement would have approximately the same stiffness as the glulam member, or twice the stiffness of the glulam member.

$$EA_{Screw} \approx EA_{Glulam}$$
$$E_{steel}\, D^2_{shaft}\, \pi / 4 \approx E_{90,mean} \cdot L_{glulam} \cdot W_{glulam}$$

(5)

Figure 11 also shows the measuring points for the moisture content measuring near the end grain (SH = Stirnholz) and in the centre of the specimen (MI = Mitte). Deformations were measured on the side surfaces and on both sides as indicated with DM. The measurements were taken along the depth of the specimens in segments at the top (OB = Oben), centre (MI = Mitte) and bottom (UN = Unten).
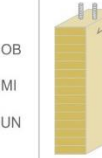

Climate scenario	unreinforced unsealed	unreinforced unsealed	unreinforced sealed	unreinforced sealed	reinforced unsealed	reinforced unsealed	reinforced sealed	reinforced unsealed	reinforced sealed
Cross section	160/160/600 mm	160/320/600 mm	160/320/600 mm	160/320/1000 mm	160/160/600 mm	160/320/600 mm	160/320/600 mm	160/320/600 mm	160/320/1000 mm
	Reference	*Reference*	*Reference*	*Reference*	$EA_{screw} \approx 2\, EA_{glulam}$	$EA_{screw} \approx EA_{glulam}$	$EA_{screw} \approx EA_{glulam}$	$EA_{screw} \approx 2\, EA_{glulam}$	$EA_{screw} \approx EA_{glulam}$
A	# P9	# P10	# P23	# P24	# P1	# P2[1]	# P3[1,3], P11[1], P12	# P4	# P13[1], P14
B			# P25	# P26	-	-	# P15[2], P16	-	# P17[2], P18
C			# P27	# P28	# P5	# P6[1]	# P7[1,3], P19[1], P20	# P8	# P21[1], P22

[1] Measurment of moisture content in depths of 15 and 40 mm
[2] Measurment of moisture content in depths of 15, 25, and 40 mm
[3] Measurment of moisture content at position SH for #P3 and #P7

Figure 11: Overview of experimental test program (the green surfaces mark sealed front faces; # P is the specimen's name; SH (Stirnholz = end grain) and MI (Mitte = centre) shows position of moisture content measurements; and DM OB , DM MI, DM UN show the reference points for the measuring of the deformation of the test specimen across the depth)

3.2 Climatization of test specimens

The ambient climate at structural members depends on the building occupation, their use, the meteorological conditions, local topography or environment, and altitude and varies throughout the year as shown in Chapter 2 Basic principles for the research project. Three stepwise climate changes were used for the experimental test programme considering sudden drying climate changes experienced by the wood before or after reinforcing. At this stage a single wetting scenario from production condition at around 65 %RH (12.1 M%) to an outdoor climate of 85 %RH (18.1 M%) was not desired by the expert committee of engineers within this project. The start of the following step drying climate considered is related to the moisture content of 12 M% from the production phase.

▸ In climate scenario A, the climate change represents the reinforcement of the timber member during production directly going into service as in the sports hall with a drying/desorption process.
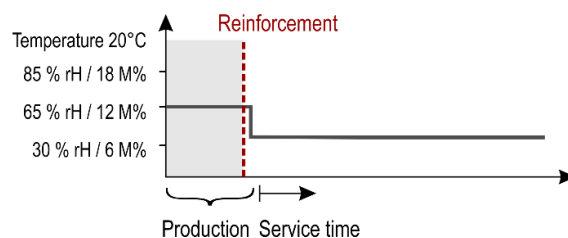
Climate scenario A

▸ The climate scenario B also represents a reinforcement of the timber member during production but going into a construction period of 38 days with wetting/adsorption process before starting service time with a drying/desorption process.
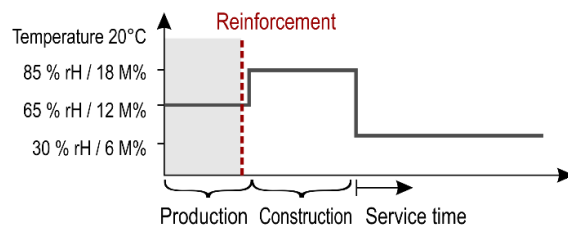
Climate scenario B

▸ In the last climate scenario C, the reinforcement is installed on-site at the end of the construction period of 38 days, followed by service with a drying process. This results in a higher moisture load after reinforcing.

Climate scenario C
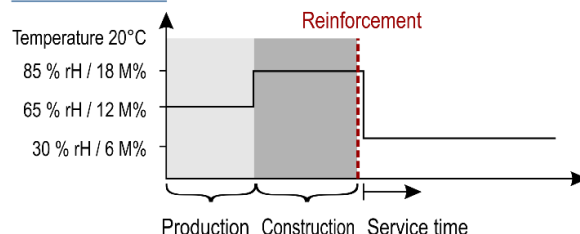
For the drying climate in scenario A, the production conditions are assumed to 65 %RH (12.1 M%) and the indoor climate to 30 %RH (6.2 M%). For the varying climates in scenario B and C, before and after reinforcing, wetting conditions with 85 %RH (18.1 M%) are applied. The following indoor climate was set to 30 %RH together with the expert committee of engineers. These mentioned relative humidity of even 10 %RH in gable roofs and behind glass facades. The relative humidity of 30 %RH can still be simulated in climate chambers. The dry climates are known to lead to cracks perpendicular to grain (Sjödin, Danzer 2020).

The elements were climatized in climate chambers. The preconditioning could be performed in smaller climate chambers (volume 0.4 m³). The tests were performed in large climate chambers (several m³), used for testing insulation properties of doors and windows: the two- and three-segment climate chambers.

3.3 Instrumentation and Measurements

3.3.1 Relevant parameters within the experimental test series

The load bearing and deformation behaviour of the test specimens under the different climatic scenarios was measured with the following parameters:

- ▸ Moisture content variations
- ▸ Deformations
- ▸ Strains

Figure 12 presents an overview of the measurement techniques applied and the following sections explain the state of the art and choice for the methods and corresponding accuracies.

3.3.2 Moisture content measurement

3.3.2.1 State of the art

Moisture content of wood can be determined using different methods of which the electrical resistance method and the sorption method (measurement of climate in a void) are the most common (Forsén and Tarvainen, 2000, Birschke et al. 2008, Franke et al. 2014, Dietsch et al. 2015, Melin et al. 2016) (Figure 13). The accuracy of the electrical resistance method depends amongst others on the species and lies between 1 M% to 2 M% (Forsén and Tarvainen, 2000). Measurement errors due to material density, distance between the gauges, type of gauges is small, but those caused by temperature are to be corrected for (Figure 14). Measuring moisture content below -5 ˚C is not recommended and considered unreliable below -10 ˚C (Fortino et al., 2016). The electrical resistance method also allows measurement of moisture content above fiber saturation point and requires the use of a relative humidity sensor in a small cavity/bore hole in the wood (Figure 15). The sorption method is not limited to a certain range of temperature (Melin et al. 2016 and Dyken and Kepp, 2010). The main drawback of the method is that it does not allow
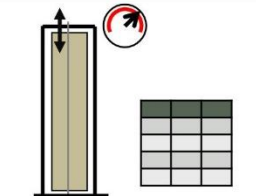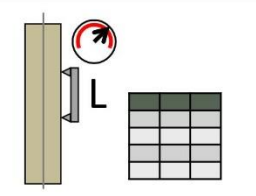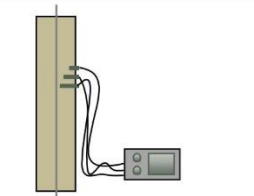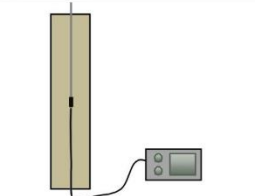
Measurand	Displacement (global)	Displacement (local)	Moisture content	Strain (local)
Methode	Dial gauge	Deformeter	Electrical resistance	Strain gauges
Range/ Position	670, 1070 mm	100, 200 mm	15, 25, 40 mm	290 mm depth
Accuracy	0.01 mm	0.001 mm	1-2 M%	Micro strain
Photo				
Principal Sketch				

Figure 12: Overview of used measuring techniques in the experiments

measurement of moisture above the fibre saturation point. Extensive monitoring campaigns on bridges have also been performed using the sorption method. It is considered more accurate than the electrical resistance method, but measurement errors can easily occur with rapid or large temperature variations (Norsk Treteknisk Institut, 2013).
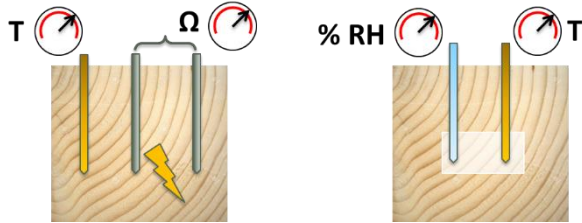
Figure 13: Illustration of moisture content measurement using the resistance method (left) where resistance and temperature needs to be measured and the measurement of climate within a small void (right) where relative humidity and temperature is measured

Figure 14: Partially Teflon coated GANN electrodes (left), partially insulated screws (middle) and CMOS relative humidity and temperature sensor (right).

3.3.2.2   Moisture measurement equipment

The electrical resistance method was used to measure moisture content in the glulam beams. Electrical resistance was measured using the Scanntronik Gigamodul and the data was logged using the Thermofox or Hygrofox produced by Scanntronik Mugrauer GmbH. Partially insulated GANN electrodes were used (Figure 15). Measurements were logged every hour. Electrical resistance is converted to moisture content using methods published by Forsén and Tarvainen (2000). Material temperature measured in the structural elements is used to compensate for temperature effects. Moisture content U is expressed in mass percentages (M%) and R is input in Ohms (Figure 15).

$$u = \frac{\log(\log(R) - 5) - f_2}{f_1} \tag{6}$$

Where parameters f_1 = -0.036 and f_2 = 1.040. Temperature effects are compensated for by using the measured moisture content U and parameters f_1 and f_2.

$$u_{temp} = \frac{0.00147 \cdot T \cdot \ln(10) + \ln\left(e^{f_1 u \ln(10) + f_2 \ln(10)} + 1\right) - 1.075 \ln(10)}{\ln(10)\left(0.000158T + 0.0262\right)} \tag{7}$$

Expected equilibrium moisture contents were calculated using the Simpson equation where φ is relative humidity and T is temperature in ˚C. A comparison of the mathematical equations to experiments (Hedlin, 1968 and Hansen, 1986) is made in Figure 16. The measurement of climate in the climate chambers was performed with calibrated Elprolog TH1 sensors. Measurements were logged typically every 10 minutes.

$$u_{EMC} = \frac{1800}{M_p}\left(\frac{K_1\varphi}{1 - K_1\varphi} + \frac{K_2 K_1\varphi + 2K_3 K_2 K_1^2\varphi^2}{1 + K_2 K_1\varphi + K_3 K_2 K_1^2\varphi^2}\right) \tag{8}$$

In which the temperature dependent parameters are calculated using:

$$M_p = 349 + 1.29T + 1.35 \cdot 10^{-2} T^2$$
$$K_1 = 0.805 + 7.36 \cdot 10^{-4} T - 2.73 \cdot 10^{-6} T^2$$
$$K_2 = 6.27 - 9.38 \cdot 10^{-3} T - 3.03 \cdot 10^{-4} T^2$$
$$K_3 = 1.91 + 4.07 \cdot 10^{-2} T - 2.93 \cdot 10^{-6} T^2$$

(9)
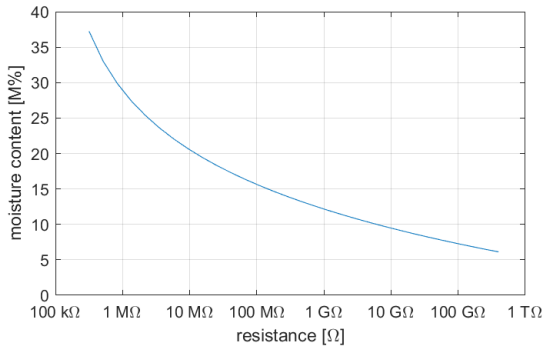
Figure 15: Relation between resistance and moisture content (Forsén and Tarvainen, 2000)
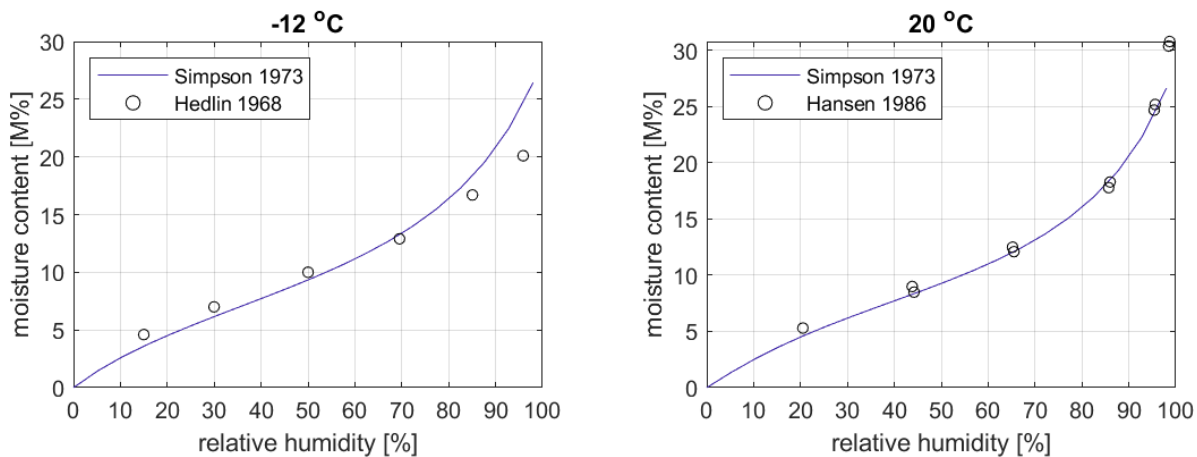
Figure 16: Mathematical formulation for equilibrium moisture content of wood and the comparison to experiments at -12 ˚C and 20 ˚C (Hedlin 1986 and Hansen 1986)

3.3.2.3   Accuracy of the moisture measurements

The used material in the glulam members is Spruce. The accuracy of the electrical resistance method lies around 2 M% (Forsén and Tarvainen, 2000).

3.3.2.4   Instrumentation

Electrode pairs were used to measure moisture content changes in the elements, cp. Figure 17. The used lengths of the electrode pairs were 15 mm and 40 mm. Elements climatized in climate B were additionally instrumented with 25 mm long electrode pairs.

The individually number of electrodes per specimen elements is as followed:

- ▸ # P2, P3, P6, P7, P11, P13, P19, and P21 were each instrumented with 4 electrode pairs, result-ing in 32 moisture content measurements.
- ▸ # P15 and P17 were instrumented with 6 electrode pairs each, resulting in a total of 12 moisture content measurements.

The measurement points were given the names according to the element number, the type of measure-ment, the location, and the length of the electrode:

- ▸ Px, specimen element name
- ▸ HF, moisture content (Holzfeuchte)
- ▸ MI or SH, centre lengthwise (Mitte) and end grain (Stirnholz)
- ▸ 15, 25, or 40, electrode length resp. measuring depth in mm

E.g., the name P3-HF-MI-15 stood for the moisture content measurement, mid-section in 15 mm depth of the element P3.
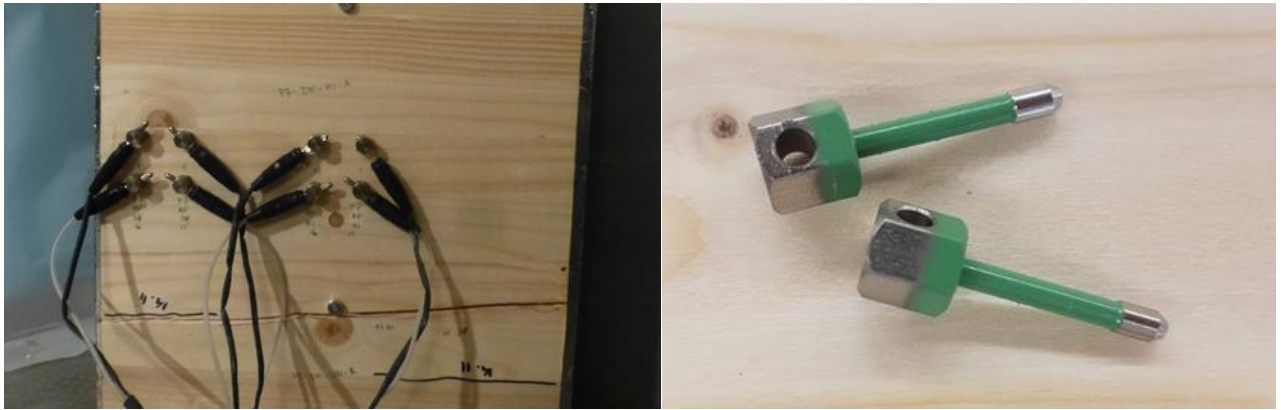
Figure 17: Pictures of the electrode pairs in the elements (P7) measuring moisture contents in two depths, in the centre of the elements and close to the end grain. On the right there is a picture of the 15 mm long elec-trodes.

3.3.3   Deformations

3.3.3.1   Deformation of the reinforcement

The deformations are measured on a relative level. Figure 12 illustrated two different methods: (1) A frame with a meter on top to measure the deformation of the reinforcement and (2) a deformeter to measure relative displacement over a length of 100 mm and 200 mm, see chapter 3.3.3.2.

To estimate the expected deformation of the height of the reinforcement, the following equations are used. The equations are more elaborately discussed in Section 4. The stress in a cross section in con-strained swelling and shrinkage is:

$$\sigma = \varepsilon \cdot E = \alpha/2 \cdot \Delta u \cdot E \tag{10}$$

Where the hygro-expansion factor α is divided by two to consider material relaxation due to constrained swelling [Danzer et al., 2020]. The material elasticity E ($E_{t,90,m}$ =300 N/mm²) and hygro-expansion factor α_{90} (0.25 %/M%) are obtained from the SIA 265 (2012) and SIA 265/1 (2018). The moisture content corre-sponding to a maximum tensile stress σ ($f_{t,90,c}$ = 0.5 N/mm², SN EN 14080, 2013) is calculated by rewriting equation (10):

$$\Delta u = 2\sigma/\alpha E = 2 \cdot 0.5/0.0025 \cdot 300 = 1.3 \, \text{M\%} \tag{11}$$

The strain and height of the glulam beam is used to calculate the deformation of the beam:

$$\delta = \varepsilon H = \alpha \cdot \Delta u \cdot H = 0.0025 \cdot 1.3 \cdot 600 = 1.95 \text{ mm} \tag{12}$$

Where *H* represents the height of the beam. To measure the deformation until fracture, a more accurate measurement is needed, say one fifth of the total deformation, i.e., 0.39 mm. The laboratories of the BFH have callipers that can measure up to 600 mm, and measurement resolution is 0.1 mm. Instead of measuring the absolute length with callipers, the option was considered to measure relative deformation. A frame was constructed for this purpose where the glulam beams would fit in Figure 18.

On the top of the frame a gauge was fixed that had a measuring range of 10 mm with a 0.01 mm measuring resolution. This gauge was mounted above a slotted plate which was fixed on the top of the frame. The bottom of the frame was fitted with a bolt in which the screw reinforcement would be fit. A small hole in the bottom of the threaded bar was drilled for this purpose. These two fixed ensured the glulam beam was always inserted in the same way and that the measurement could be made while the beam was in a vertical position.

The measurements could not be performed in a continuous manner. Shortly after climate in the climate chamber was changed, deformations would be measured with a frequency of two to three days. As time progressed, these measurements were made on intervals of one week as deformations did not change much over time anymore. Before and after each measurement, the length of a reference bar was measured. An example is shown of the variations are plotted in Figure 19. The reference bar for the 600 mm high glulam beams was named R670, that for the 1000 mm high beams was named R1070. The bars were 70 mm longer than the beam height to fit these into fixed position in the measuring frames.

The frame was made of aluminium ITEM profiles. Although the frames remained in the climate chambers during the climatization of the glulam beams and temperature was not changed, measurement error due to thermal expansion was possible. A relative elongation due to thermal expansion can be estimated using the thermal expansion factors, like the one used in Equation (12).
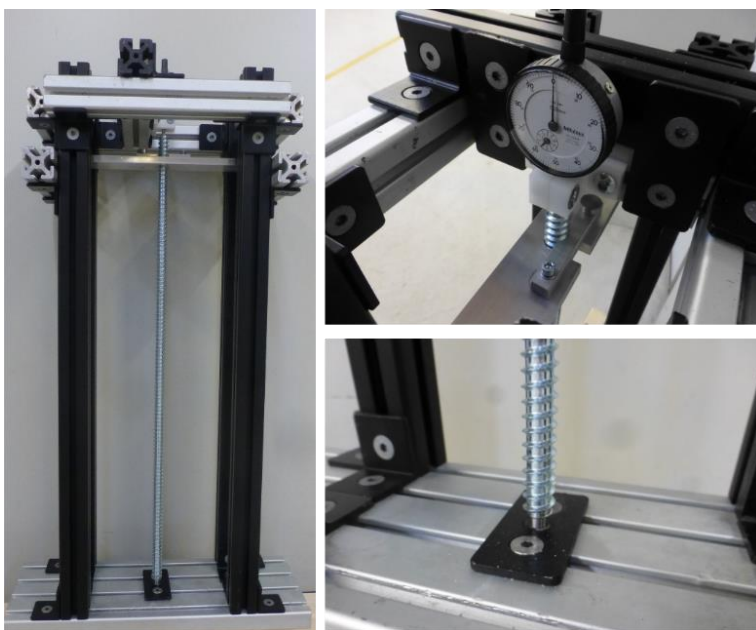
Figure 18: Picture of the constructed frame to measure 600 mm high beam with a gauge at the top and a nut to fit the screw into on the bottom. A similar frame was constructed for the 1000 mm high glulam beams.
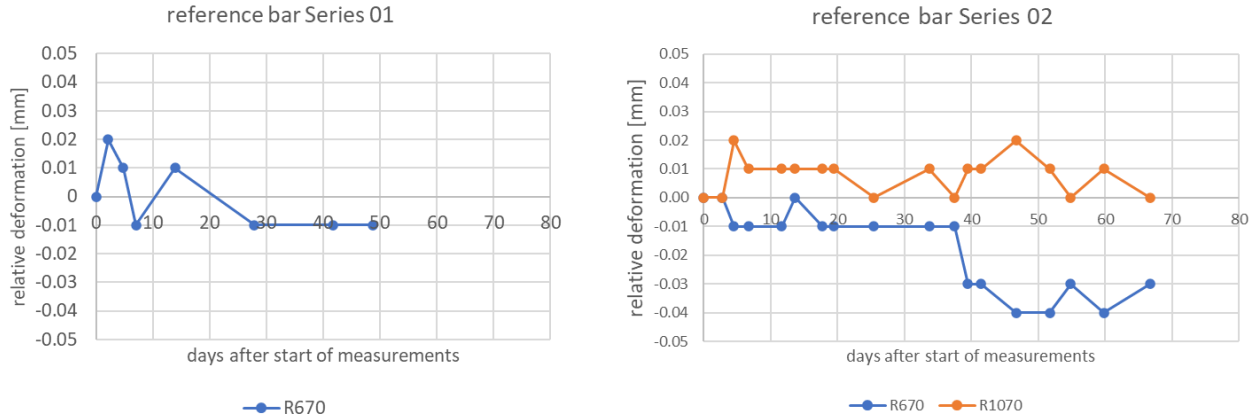
Figure 19: Measured relative deformations of reference beams R670 and R1070.

$$\delta_{R670} = \left(\beta_{steel} - \beta_{alu}\right)\Delta T \cdot l_{R670} = \left(17.3 - 20\right)\cdot 10^{-6}\cdot 1 \cdot 670 = -0.0025 \text{ mm}$$
$$\delta_{R1070} = \left(\beta_{steel} - \beta_{alu}\right)\Delta T \cdot l_{R1070} = \left(17.3 - 20\right)\cdot 10^{-6}\cdot 1 \cdot 1070 = -0.0040 \text{ mm}$$

(13)

The reference bar can deform freely. In case of small temperature variations, deformations in the range of a couple of micrometres can be expected. The resolution of the used gauge is 0.0100 mm. Once the steel deformation is constraint (by the glulam), the measurement errors are larger. These lie within the measurement resolution of the gauge but remain small (order of 1/100th of a millimetre).

$$\delta_{R670} = \left(\beta_{steel} - \beta_{alu}\right)\Delta T \cdot l_{R670} = \left(0 - 20\right)\cdot 10^{-6}\cdot 1 \cdot 670 = -0.0134 \text{ mm}$$
$$\delta_{R1070} = \left(\beta_{steel} - \beta_{alu}\right)\Delta T \cdot l_{R1070} = \left(0 - 20\right)\cdot 10^{-6}\cdot 1 \cdot 1070 = -0.0214 \text{ mm}$$

(14)

3.3.3.2   Deformation of the glulam beam

The second method to measure deformation was by using the deformeter. The system functioned like the frame, other that deformations over distances of 100 mm to 200 mm were measured (Figure 20). Bolts with a small, drilled hole in the middle were glued onto the surface of the glulam beams as reference points. The deformations were measured each time the deformations were also measured on the rein-forcements. Before each measurement, the deformeter was be calibrated.
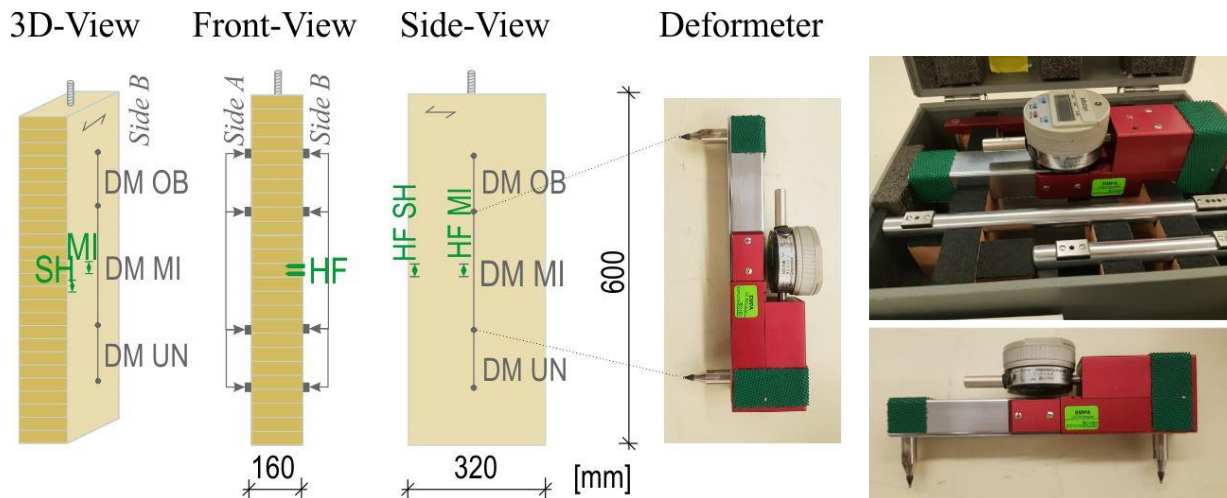
Figure 20: Illustration of the measurement of deformations on the surface of the 1000 mm glulam beam (left) using the deformeter (bottom left) which was calibrated before each measurement using the fixed bars with 100 mm or 200 mm distance

The uncertainty interval of these measurements was not estimated. However, measurements made on both side of the beams (A-side and B-side) were averaged. It is known in experimental strain measurements that axial strains should be measured on both sides of an axially loaded element. An eccentricity in loading of 10 % of the square (width b and height h) height leads to a measurement error of 60 % if strains are measured on one side only.

$$\varepsilon_{\pm h/2} = \frac{F}{AE} \pm \frac{My}{IE} = \frac{F}{AE} \pm \frac{0.1hF\,0.5h}{IE} = \frac{F}{E}\left(\frac{1}{bh} \pm \frac{12h^2}{20h^3b}\right) = \frac{F}{Ebh}(1 \pm 0.6) \qquad (15)$$

In other words, either 40 % of the strain or 160 % of the strain is measured. Averaging these two strains results in a representative strain. The same holds for measurement of the displacements. An asymmetry in the deformation, like seen in Wallner (2012) will be averaged out.

3.3.4 Strain

3.3.4.1 Instrumentation of the screws with strain gauges

Strains were measured in the steel reinforcements by gluing a strain gauge into a 4 mm diameter hole in the screw. A 16 mm diameter screw has a 12 mm shaft diameter. Drilling a 4 mm hole in this shaft reduces the cross-section surface, and stiffness (area times E-modulus) by only 1/9th. The 4 mm hole was drilled into the screw to a depth of 290 mm using a total of four drills of different lengths.

- 70 mm
- 150 mm
- 210 mm
- 290 mm

After this, the hole was cleaned, and the gluing of the strain gauge was prepared. The used 2 mm diameter strain gauge (HBM 1-LB11-3/120ZW) was glued into the 290 mm hole using EP150 epoxy glue that was cured in temperatures around 180 ˚C for more than two hours (Figure 21).

3.3.4.2 Expected accuracy of the strain measurement

The strain gauge HBM 1-LB11-3/120ZW has a width of nearly 2 mm and is intended to be glued into a 2 mm hole. Drilling a 300 mm deep hole with 4 mm in diameter into a screw was difficult already (L/D = 75 compared to normal L/D ratio of 15), so drilling a 2 mm hole was not possible for that length. However, several preliminary tests were performed with both diameters first into smaller bars, which were then axially loaded (Figure 22).

Figure 21: Illustration of the strain gauge position (DMS) in the glulam beam and pictures of the preparation process of the screws
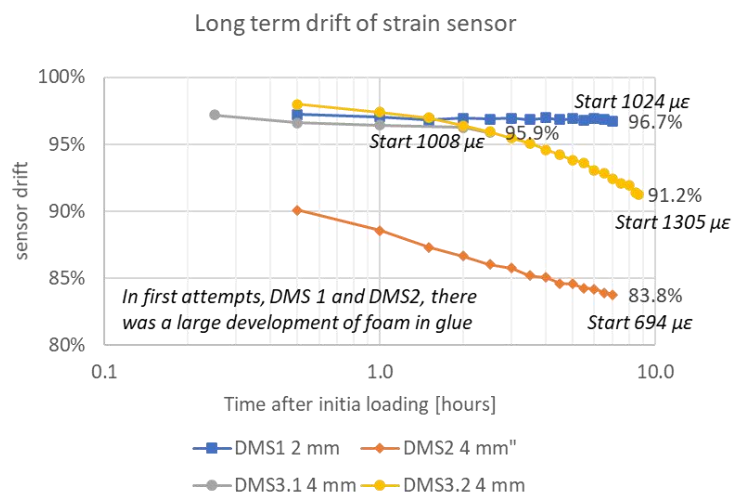
Figure 22: Experiment results intended to test the long-term stability of the strain measurements

In the first preliminary tests, a steel bar was instrumented with a strain gauge in a 2 mm diameter hole (DMS1) and a second in a 4 mm diameter hole (DMS2), see Figure 22. The EP150 glue foamed significantly duri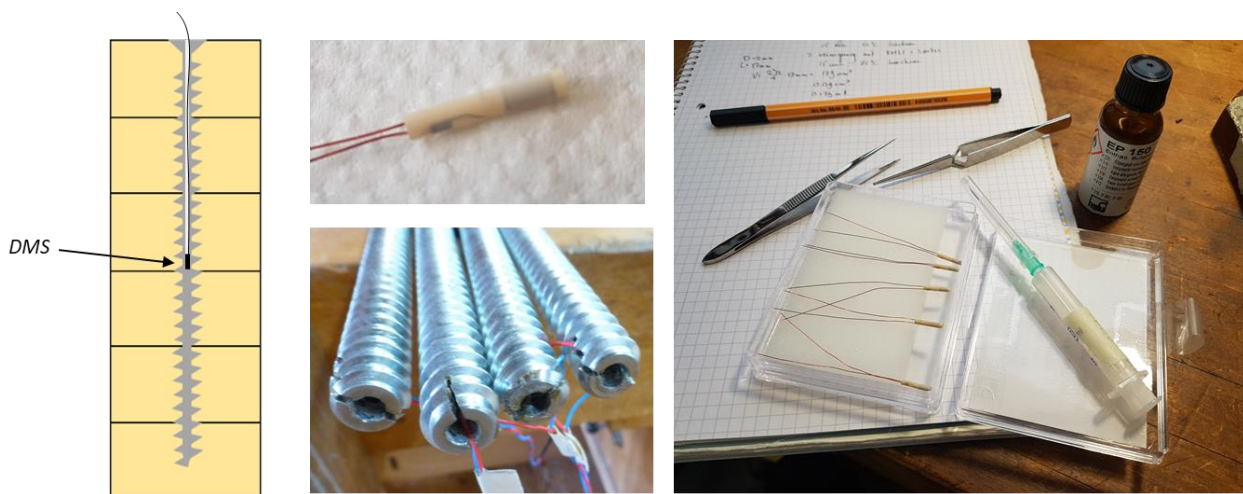ng its curing which was accredited to small air bubbles in the glue, likely created during the shaking of the glue prior to its gluing. Both hole depths were 60 mm. The rod could axially be loaded by using nuts, washers, and a tube. The instrumented bar was put into the steel tube after which the nuts were tightened onto the washers and tube, creating a tension load on the instrumented bar, and a compression load on the tube. This created an equal amount of strain on both gauges (DMS1 and DMS2)

Long term performance of the DMS2 strain gauge was dramatic compared to the DMS1. Whereas the DMS measured a 1024 micro strain at the start of the experiment, the DMS2 only measured 694 micro strains. Over the course of 8 hours, the reduction of strain was in DMS1 was only 3 % and that in the DMS2 reduced 16 %. Over 8 hours measurement time DMS2 measured roughly 57 % (=694/1024 · 0.83) less 'force' than the DMS1.

In a second gluing test (DMS3), the EP150 adhesive was stirred prior to the gluing to reduce the amount of air bubbles. Only a small of amount of foaming occurred in in the 4 mm diameter hole. The bar was loaded again an at a start value of 1008 micro-strain only 5 % error was measured after four hours (DMS3.1), and in a second test with a start strain of 1305 micro-strain, 9 % error was measured after nearly 10 hours (DMS3.2). This high value of micro-strain would, in the steel screw reinforcement, correspond to an axial load of 31.0 kN in a 16 mm screw. A value which was unlikely to be reached in climatization tests. The extreme high loading is also expected to be the cause of the continuously increasing creep in the DMS3.2 test. For short term tests, for instance to test reinforcement of a notch or a hole in a glulam beam, the applied procedure to glue the strain gauges in the screws can result in reliable values.

The measurement error due to a deviation of the bore hole at 300 mm depth was also performed. This is due to the likelihood of the drill not staying in the exact centre of the screw (Figure 23). In this calculation, the parameter *e* represents the eccentricity of the hole and the gauge. Due to this eccentricity, the neutral axis shifts outward, and a (pinned supported) bar will not only elongate, but also bend. The area, moment of inertia, and location of the neutral axis are calculated using the following equations.

$$A = \frac{D^2 \pi}{4} - \frac{d_i^2 \pi}{4} = \frac{\left(D^2 - d_i^2\right)\pi}{4} = \frac{\left(12^2 - 4^2\right)\pi}{4} = 32\pi$$

$$I = \frac{D^4 \pi}{32} - \left(\frac{d_i^4 \pi}{32} + \frac{d_i^2 \pi}{4} \cdot e^2\right) = \frac{\left(D^4 - d_i^4\right)\pi}{32} - \frac{d_i^2 \pi}{4} \cdot e^2 = \frac{64340}{32}\pi - 4\pi e^2 = 640\pi - 4\pi e^2 \qquad (16)$$

$$na = \frac{\dfrac{D^2 \pi}{4} \cdot 0 - \dfrac{d_i^2 \pi}{4} \cdot e}{\dfrac{D^2 \pi}{4} - \dfrac{d_i^2 \pi}{4}} = \frac{-d_i^2 \pi e}{\left(D^2 - d_i^2\right)\pi} = -\frac{1}{32}e$$

Where D is the outer diameter and d_i is the inner diameter. The strain in the centre of the drilled hole is then calculated as a function of the eccentricity. Note that the distance of the centre of the hole to the neutral axis is used to calculate the contribution of the bending moment to the strains.

$$\sigma = \frac{F}{A} + \frac{M\left(e - na\right)}{I} \longrightarrow \varepsilon = \frac{F}{EA} + \frac{M\left(e - na\right)}{EI}$$

$$\varepsilon = \frac{F}{EA} + \frac{F\left(e - na\right)^2}{EI} = \frac{F}{E}\left(\frac{2}{A} + \frac{\left(e - na\right)^2}{I}\right) \qquad (17)$$

$$\varepsilon = \frac{F}{EA} + \frac{F\left(e - na\right)^2}{EI} = \frac{F}{E}\left(\frac{2}{32\pi} + \frac{\left(e + 1/32 e\right)^2}{640\pi - 4\pi e^2}\right) = \frac{F}{E}\left(\frac{2}{32\pi} + \frac{\left(33/32\right)^2 e^2}{640\pi - 4\pi e^2}\right)$$

An eccentricity of 1 mm leads to an error of 2.7% in strain, an eccentricity of 2 mm leads to an error of 11.2 %, an eccentricity of 3 mm leads to an error in measured strain of 70.1 %. That is if, the bar is simply supported at the ends. In the climatizations of the glulam beams, the screw will follow the deformation of the glulam beam. Any curvature of the glulam beam is followed by the screw.

Finally, the measured strain was compared to the expected strain. The screws were loaded to a level of 10 kN in a universal testing machine. The average deviation of the strains on the five screws was -18 % of the expected strain. The result is difficult to interpret, keeping in mind that a small eccentricity in loading or cross section already leads to a large measurement error. The spread (standard deviation) of the measurement error is 27 %, meaning that 67 % of the values lie between +9 and -45 % of the expected strain. In is, for the moment assumed that there is a good chance the measured strain is about 18 % underestimated on average.
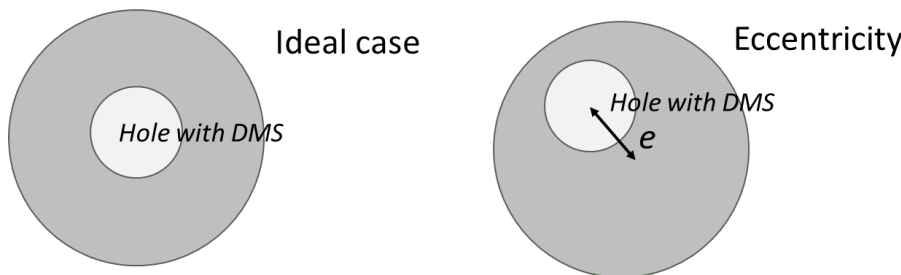

Figure 23: Illustration of the deviation of the hole and the calculation of the theoretical error in measured strain

4 Analytical analysis of hygro-expansion behaviour

4.1 Simplified numerical model for the hygro-expansion of reinforced elements

Any material with a higher stiffness than the stiffness of the base material can attract more stress when loaded. The principle is explained using a simple example with two materials with different cross sections and different materials, i.e., stiffnesses. The two materials act as a composite with full composite action and are loaded by an external force *F*.
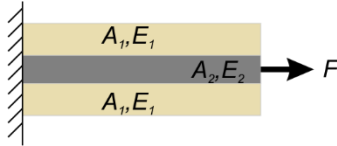
Figure 24: A composite structure consisting of two different materials 1 and 2

The total load is

$$F = \sigma_1 A_1 + \sigma_2 A_2 = \varepsilon_1 E_1 A_1 + \varepsilon_2 E_2 A_2 \,. \tag{18}$$

In a composite material, the axial strain in the two materials is the same.

$$\varepsilon_1 = \varepsilon_2 = \varepsilon_0 \rightarrow F = \sigma_1 A_1 + \sigma_2 A_2 = \varepsilon \left(E_1 A_1 + E_2 A_2 \right) \tag{19}$$

In a situation where one of the materials is either affected by a temperature change, or in this case a moisture content change, a thermal- or hygro-expansion factor should be considered, respectively. Mechano-sorptive creep and time-dependent creep, too:

$$\varepsilon_T = \varepsilon_E + \varepsilon_{HS} + \varepsilon_{MS} + \varepsilon_c \,, \tag{20}$$

where ε_T is the total strain, ε_{HS} is the hygro-sorptive strain, ε_{MS} is the mechano-sorptive strain, and ε_C is the creep strain. The mechano-sorptive strain and the creep strain are relaxation strains and are moisture, temperature, and stress dependent. These will be neglected for the moment and the focus will remain on the elastic and hygro-sorptive component.

The change of the strain or change of stress due a change of moisture content can be calculated using the following equation.

$$\Delta \varepsilon = \Delta \sigma / E + \alpha \Delta u$$
$$\Delta \varepsilon E = \Delta \sigma + \alpha \Delta u E \tag{21}$$
$$\Delta \sigma = \left(\Delta \varepsilon - \alpha \Delta u \right) E$$

Once an external force is also applied, the equation changes again. If subscript 1 is used for wood and subscript 2 is used for the steel reinforcement, the following is formulated to calculate the elastic strain:

$$\Delta \varepsilon_0 (A_1 E_1 + A_2 E_2) - \alpha_1 \Delta u_1 A_1 E_1 = F_e$$
$$\Delta \varepsilon_0 (A_1 E_1 + A_2 E_2) = F_e + \alpha_1 \Delta u_1 A_1 E_1 \tag{22}$$
$$\Delta \varepsilon_0 = \left(F_e + \alpha_1 \Delta u_1 A_1 E_1 \right) / (A_1 E_1 + A_2 E_2)$$

This can be used again to calculate the stress in the timber cross section and in the steel bar:

$$\Delta \sigma_1 = \left(\Delta \varepsilon_0 - \alpha_1 \Delta u_1 \right) E_1$$
$$\Delta \sigma_2 = \left(\Delta \varepsilon_0 - 0 \right) E_2 = \Delta \varepsilon_0 E_2 \tag{23}$$

Integrating the last line of Equation (22) into (23) allows to calculate the stress in the timber cross section in one equation:

$$\Delta\sigma_1 = \big((F_e + \alpha_1\Delta u_1 A_1 E_1)/(A_1 E_1 + A_2 E_2) - \alpha_1\Delta u_1\big)E_1$$
$$\Delta\sigma_2 = (F_e + \alpha_1\Delta u_1 A_1 E_1)/(A_1 E_1 + A_2 E_2)E_2$$

(24)

If the external force F_e is zero, the equation simplifies somewhat. If the stiffness of the steel reinforcement equals that of the timber cross section, the latter equation can be rewritten into:

$$\Delta\sigma_1 = \big((0 + \alpha_1\Delta u_1 A_1 E_1)/(A_1 E_1 + A_1 E_1) - \alpha_1\Delta u_1\big)E_1$$
$$\Delta\sigma_1 = (\alpha_1\Delta u_1 A_1 E_1/2A_1 E_1 - \alpha_1\Delta u_1)E_1$$
$$\Delta\sigma_1 = \alpha_1\Delta u_1 (A_1 E_1/2A_1 E_1 - 1)E_1$$
$$\Delta\sigma_1 = \alpha_1\Delta u_1 (-1/2)E_1 = -\alpha_1\Delta u_1 E_1/2$$

(25)

Eventually, the maximum allowable change in moisture content if the maximum allowable stress is known:

$$\Delta u_1 = \frac{-2\Delta\sigma_1}{\alpha_1 E_1}$$

(26)

In a more general case, where the stiffness of the reinforcements and cross section are not equal, equation (26) is written as

$$\Delta u_1 = \frac{\Delta\sigma_1}{\alpha_1 E_1 (\gamma - 1)}$$

(27)

Where γ is the ratio between stiffness of the reinforcement and that of the total cross section.

$$\gamma = \frac{A_1 E_1}{A_1 E_1 + A_2 E_2}$$

(28)

4.2 Transformation of deformations on the reinforcements to loads at the midheight of the cross section

A simplified FE model is made using two materials that can independently deform from one another and are connected by a spring-type element generating a compliance composite action like the mechanism illustrated in Dietsch (2012). A simple FE element is developed to allow the modelling of a simple verification of effect of hygro-expansion, moduli of elasticity, or loading type, see in Figure 25.

For a simple bar that can only be loaded axially, the general stiffness matrix is formulated as follows:

$$\mathbf{K_{el}} = \frac{E_{el} A_{el}}{l_{el}}\begin{pmatrix} 1 & -1 \\ -1 & 1 \end{pmatrix}$$

(29)

To solve the deformations of the bar that are related to an external force, the following equation must be solved:

$$\mathbf{F} = \mathbf{Ku} \quad \rightarrow \quad \mathbf{u} = \mathbf{K}^{-1}\mathbf{F}$$

(30)

To which the thermal expansion is added to the load vector:

$$\mathbf{F} = E_{el} A_{el} \alpha_{el} \Delta T\begin{pmatrix} -1 \\ 1 \end{pmatrix}$$

(31)
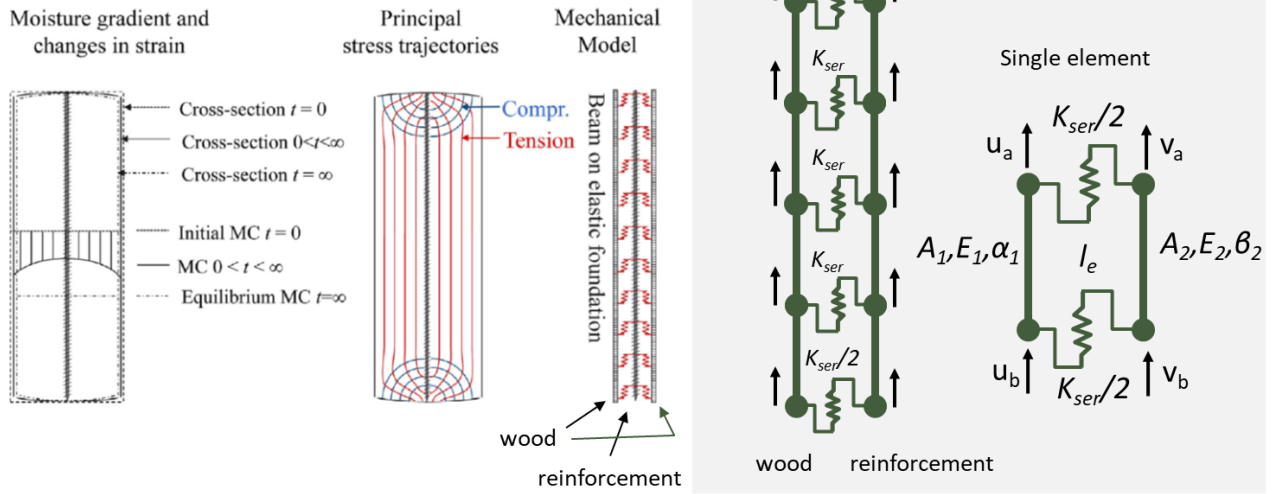
Figure 25: Simplification of the interaction between glulam and reinforcement (compliance composite action) as shown by the mechanical model in Dietsch (2012) (left) and simplified FE-model and FE element (right)

The stress following from a bar that is subjected to an external load as well as a thermal load, can then be calculated as follows:

$$\sigma = E_{el}\varepsilon_{elastic} - E_{el}\alpha_{el}\Delta T \tag{32}$$

These relations are now used to set up a stiffness matrix and a load vector for the element illustrated in Figure 25 on the right.

$$\mathbf{K}_{el} = \begin{pmatrix} \dfrac{E_1 A_1}{l_{el}} + \dfrac{K_{ser}}{2} & -\dfrac{K_{ser}}{2} & -\dfrac{E_1 A_1}{l_{el}} & 0 \\[3mm] -\dfrac{K_{ser}}{2} & \dfrac{E_2 A_2}{l_{el}} + \dfrac{K_{ser}}{2} & 0 & -\dfrac{E_2 A_2}{l_{el}} \\[3mm] -\dfrac{E_1 A_1}{l_{el}} & 0 & \dfrac{E_1 A_1}{l_{el}} + \dfrac{K_{ser}}{2} & -\dfrac{K_{ser}}{2} \\[3mm] 0 & -\dfrac{E_2 A_2}{l_{el}} & -\dfrac{K_{ser}}{2} & \dfrac{E_2 A_2}{l_{el}} + \dfrac{K_{ser}}{2} \end{pmatrix}, \qquad \mathbf{u}_{el} = \begin{pmatrix} u_a \\ v_a \\ u_b \\ v_b \end{pmatrix} \tag{33}$$

The load vector is formulated as follows, using α for the hygro-expansion of wood and β for the thermal expansion of steel:

$$\mathbf{F}_{el} = E_1 A_1 \alpha_1 \Delta u \begin{pmatrix} -1 \\ 0 \\ 1 \\ 0 \end{pmatrix} + E_2 A_2 \beta_2 \Delta T \begin{pmatrix} 0 \\ -1 \\ 0 \\ 1 \end{pmatrix} + \mathbf{F}_{ext} \tag{34}$$

The stress in the timber is then calculated as follows:

$$\sigma_1 = E_1 \frac{(u_b - u_a)}{l_{el}} - E_1 \alpha_1 \Delta u \tag{35}$$

The stress in the steel reinforcement is then calculated as:

$$\sigma_2 = E_2 \frac{(v_b - v_a)}{l_{el}} - E_2 \beta_2 \Delta T \qquad (36)$$

The beam parameters like the elasticity modulus and area can be input as wished and as they correspond to the system that needs to be simulated. The stiffness between the timber and reinforcements is obtained from the ETA-documents of the reinforcement.

$$K_{ser} = 25 \cdot D_{thread} \cdot l_{el} \qquad (37)$$

The distribution of the loads on the springs between the two materials can be calculated as follows:

$$\mathbf{V_{el}} = \frac{K_{ser}}{2} \left(\begin{pmatrix} u_a \\ u_b \end{pmatrix} - \begin{pmatrix} v_a \\ v_b \end{pmatrix} \right) \qquad (38)$$

Figure 26 to Figure 29 show the relations of fully interlocking reinforcement (full composite action) and glulam beam to the more realistic case where the stiffness of the connection and height of the beam is considered (compliance composite action). For the 600 mm high beam and 1000 mm high beam, the average strains need to be multiplied by 1.42 and 1.34 respectively to calculate the theoretical maximum strain in the centre of the reinforcement (Figure 28). This means that the loads on the cross sections (or reinforcement) of the idealized case can be reduced by almost 30% and 10% once the idealized case is considered (Figure 29).
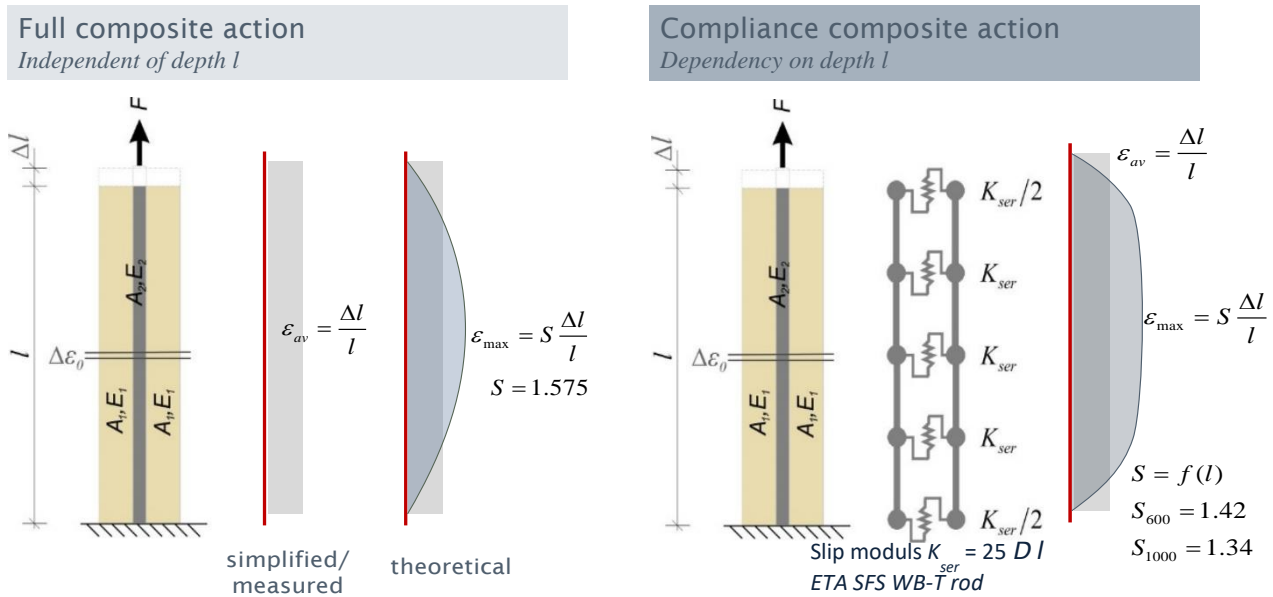
Figure 26: Comparisons and relations of average and theoretical strain distributions for full and compliance composite action models in dependency of the beam height: the higher the beam
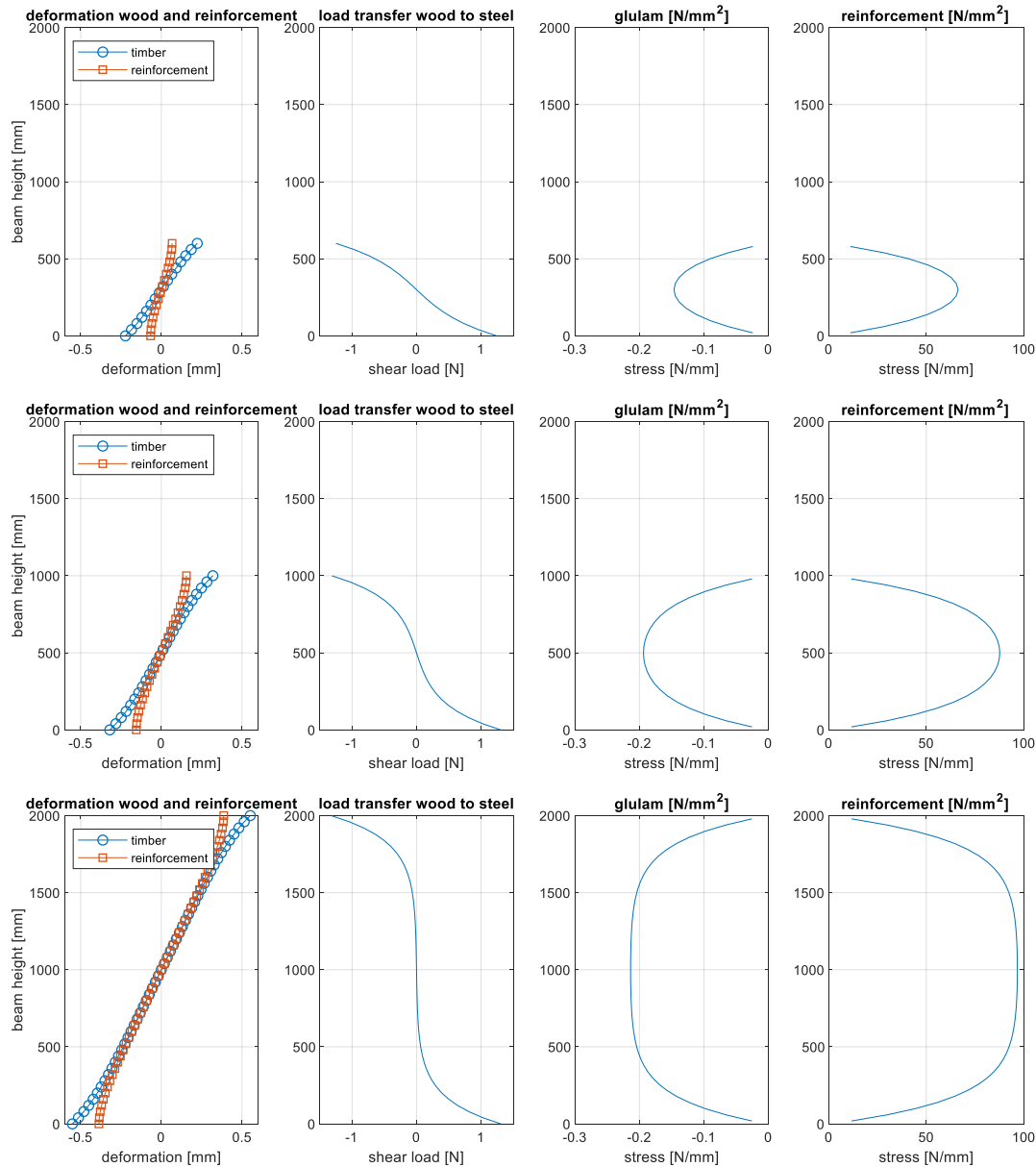
Figure 27: Deformations, shear load and stress distribution in the glulam and reinforcement for heights of 600, 1000 and 2000 mm
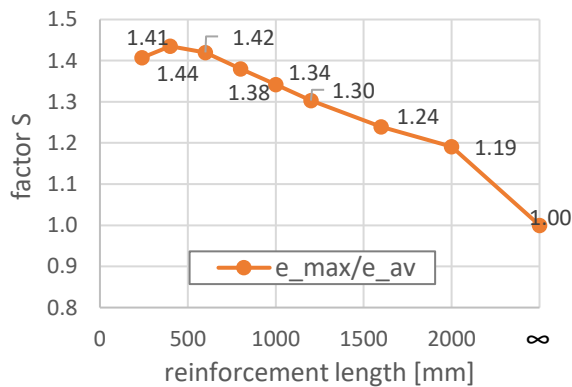
Figure 28: Relationship/factor between average strain and maximum strain for the compliance composite action model depending on the reinforcement length and infinitive heigh beam as reference
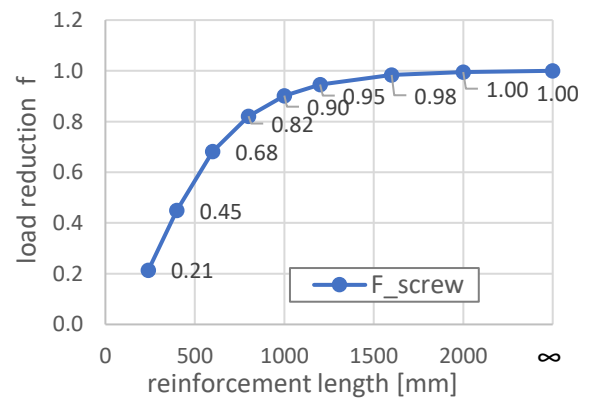
Figure 29: Reduction of load F for the compliance composite action model depending on the reinforcement length and infinitive heigh beam as reference

4.3 Validation of first model

The first model presented in Section 4.1 is validate through the calculation of some extreme cases: one where the shrinking and swelling of the timber cross section is fully constraint, and one where it is not constraint at all. To take this into account, the E2 will either me assumed to be infinite or zero, respectively.

Under full constraint, where the 'stiffness of the steel reinforcement is infinite', the gamma from equation 30 is calculated first.

$$\gamma = \frac{A_1 E_1}{A_1 E_1 + A_2 E_2} \quad \rightarrow \quad \gamma = \frac{A_1 E_1}{A_1 E_1 + A_2 \infty} = 0 \tag{39}$$

Where this is then filled in the equation 29 being:

$$\Delta u_1 = \frac{\Delta \sigma_1}{\alpha_1 E_1 \left(0 - 1\right)} = -\frac{\Delta \sigma_1}{\alpha_1 E_1} \quad \rightarrow \quad \Delta \sigma_1 = \alpha_1 E_1 \Delta u_1 \tag{40}$$

An equation also found in literature CC.

In the second case, the stiffness of the reinforcement is set to zero, and therefore the wood can deform freely. In such a case, no stresses in the wood can develop.

$$\gamma = \frac{A_1 E_1}{A_1 E_1 + A_2 E_2} \quad \rightarrow \quad \gamma = \frac{A_1 E_1}{A_1 E_1 + A_2 \cdot 0} = 1 \tag{41}$$

The allowable moisture content change is then calculated to be:

$$\Delta u_1 = \frac{\Delta \sigma_1}{\alpha_1 E_1 \left(1 - 1\right)} = -\frac{\Delta \sigma_1}{\alpha_1 E_1 \cdot 0} \quad \rightarrow \quad \Delta \sigma_1 = 0 \tag{42}$$

Which in other words says that the moisture content change is allowed to be whatever value, regardless of the parameters for stiffness and hygro-expansion factor. If it is rewritten, the equation can be read as one where the stresses in the wood will always be zero, no matter what the moisture content change is.

4.4 Comparison with an existing model

Volkersen (1938) developed a model in which the displacement of two strips joined by rivets, can be calculated. The strains in the two strips of different thicknesses can be calculated when knowing the stiffness of the connection between the two. This connection can also be a glue (Figure 30).

The displacement along the length of the connection with respect to the average displacement can be calculated as follows:

$$\frac{\delta_x}{\delta_m} = \frac{\sqrt{\Delta y}}{\sinh \sqrt{\Delta/y}} \left[\left(1/\gamma - 1\right) \cosh\left(\sqrt{\Delta/\gamma}\,\frac{x}{L}\right) + \cosh\left(\sqrt{\Delta/\gamma}\left(1 - \frac{x}{L}\right)\right) \right] \tag{43}$$

Two parameters are calculated. The first is the average displacement:

$$\delta_m = \frac{F}{b \cdot l \cdot K} \tag{44}$$

The stiffness of the connection Δ is calculated as follows:

$$\Delta = \frac{K \cdot b \cdot l^2}{E_2 F_2} \tag{45}$$

A comparison of the relative displacement between two materials connected by an elastic material as modelled with the FE modelled and the Volkersen model with a stiffness ratio γ of 0.39.
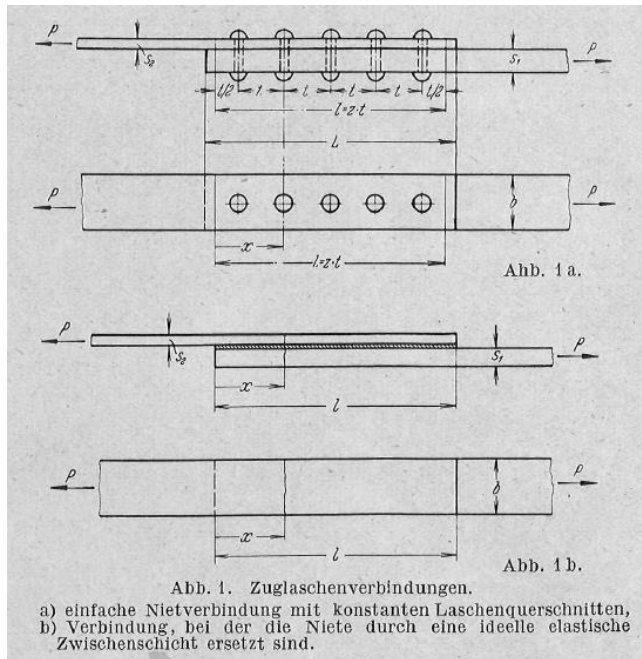
Figure 30: Illustration of the connection modelled by Volkersen (1938): above the riveted connection and below the glued connection.
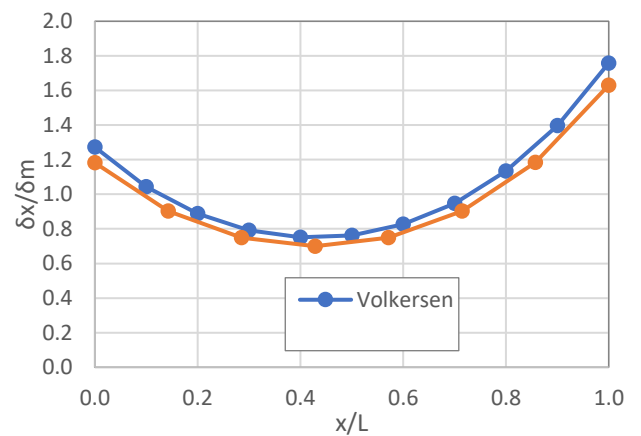
Figure 31: Comparison between relative displacement between two materials in FE-model and model as suggested by Volkersen (1938) in a stiffness ratio of 0.38.

5 Results of experimental test programme

5.1 Climate measurements during climatization after reinforcement

The measured climates for scenario A, B, and C during the climatization are shown in Figure 32. In climate scenario A, the drying climate could almost be maintained constant at about 20 ˚C and 28 % rH. During two dropouts of about 1 week each in the climate chamber (grey area) the temperature dropped down and the relative humidity increased to 40 % maximum. It is assumed, that this does not affect the results. In climate scenario B, the temperature was maintained at a constant level of 20 ˚C for both climate steps while the relative humidity was maintained at 87 % rH and about 30 % rH for the two climate steps. Similar to climate scenario A, the relative humidity in climate scenario C could not be maintained constant. It was measured to be at 35 % in the beginning and about 30 % after 17 days. However also two dropouts occurred which led to higher relative humidity afterwards. The temperature was constantly 20 ˚C.
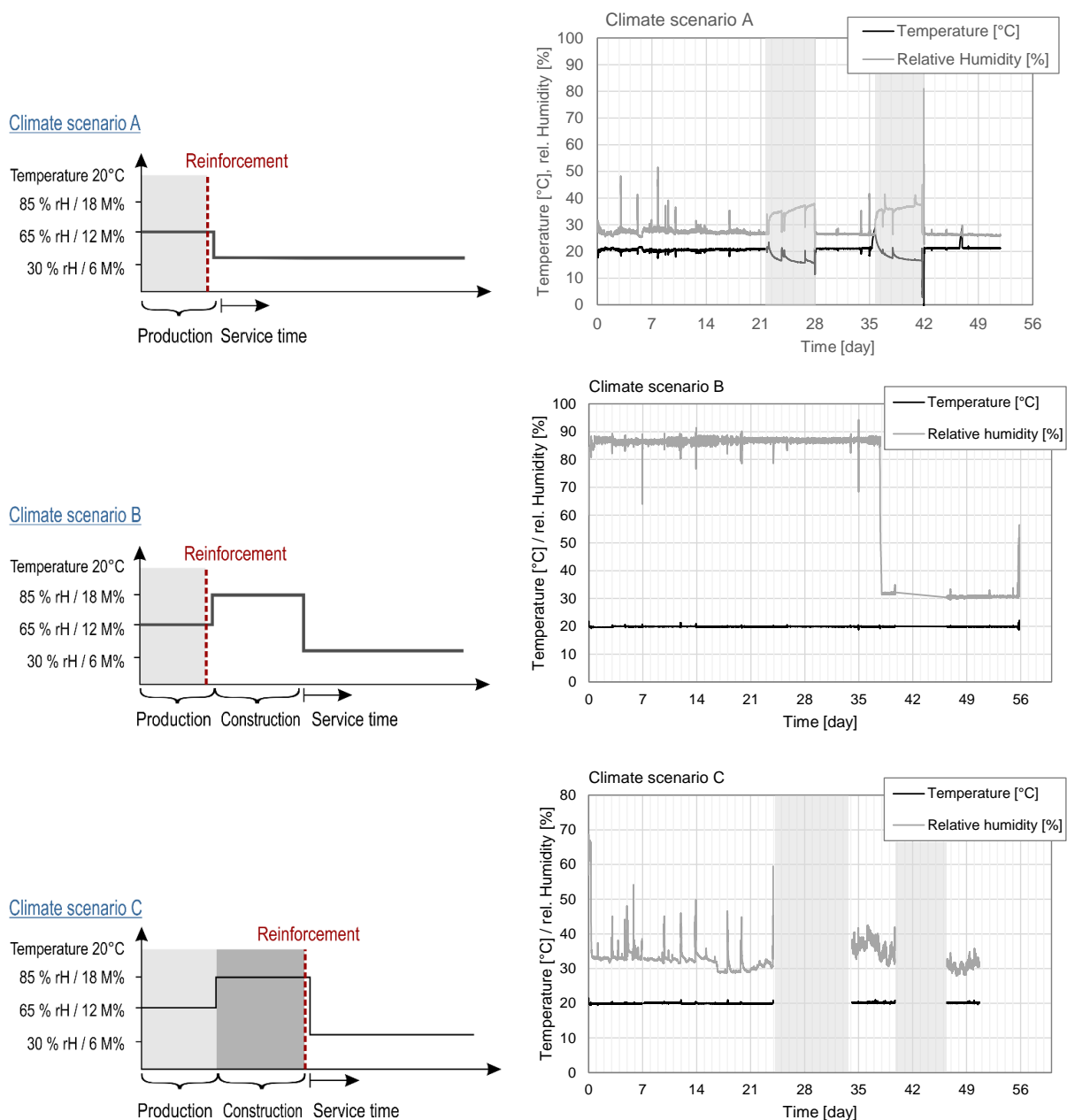
Figure 32: Measured climates during the climatization of the specimen after reinforcement, grey marked time represents drop-off of climate chamber or data logger

5.2 Moisture content measurements

5.2.1 Overview over complete test programme

The moisture content measurements are shown in Figure 33 for all test specimen and climate scenarios summarised for the unsealed specimen on the left and the sealed specimen on the right. The 1000 mm high specimens are always marked as green lines. As can be seen, not all specimens start with the intended moisture content after the pre-climatization (before reinforcement). The intended pre-climatization of the elements P2, P3 and P6, P7 to a moisture content of 12 M% and 18 M% was not achieved. Instead, the climatization was achieved at levels between 10 M% and 12 M%. The relative humidity in one climate chamber was too low. Elements in the second climate chamber were not stored long enough to achieve the aimed moisture content in time.

The pre-climatization of the second series P19 and P21 was redesigned. To achieve the moisture content of 18 M%, the elements were stored in a climate chamber with a relative humidity of 85%. Instead of
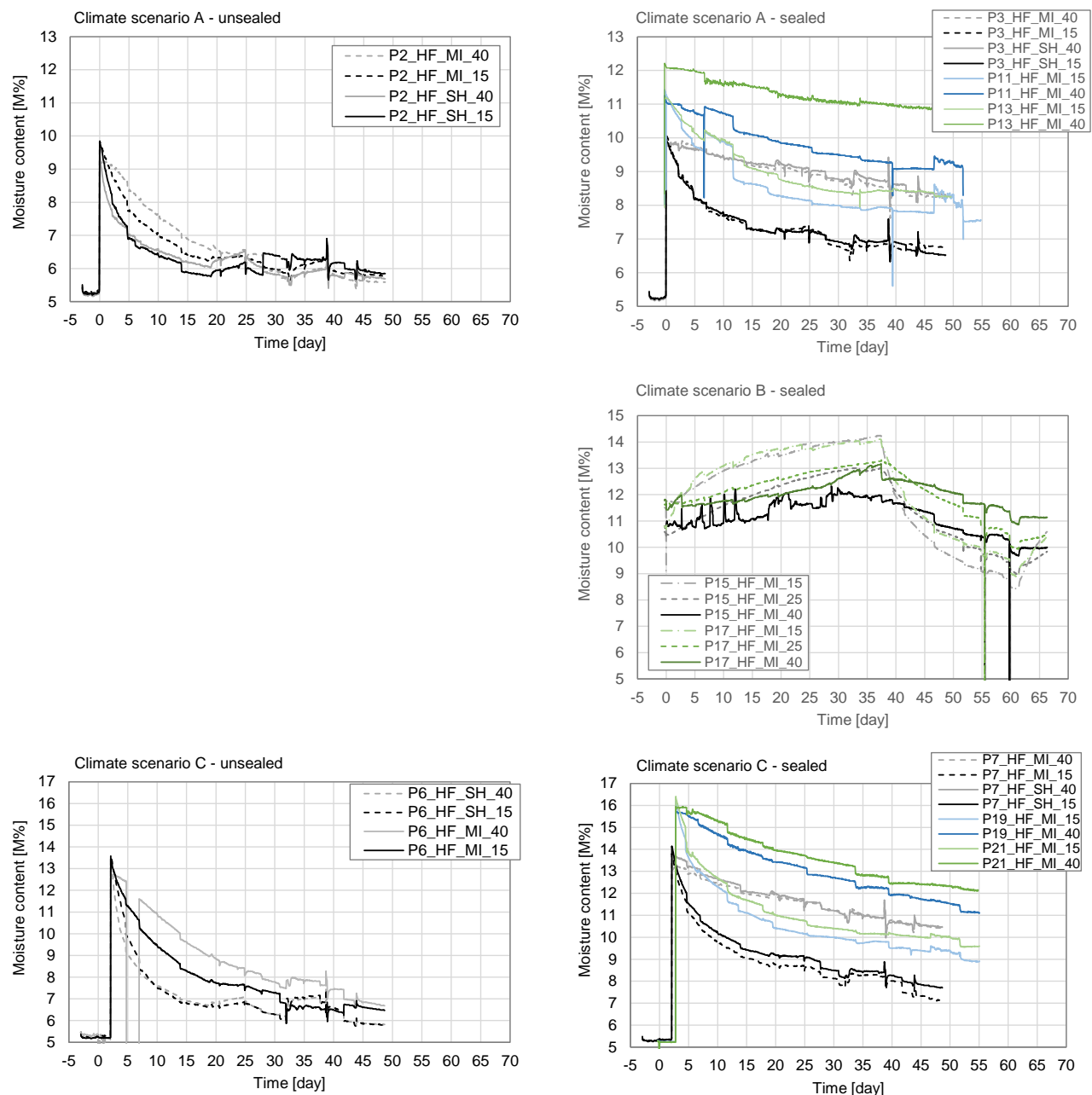
Figure 33: Moisture content measurements for all three climate scenarios, the unsealed specimen (left) and sealed specimens (right)

maintaining the temperature at 20 °C, like was done in the first series, a higher temperature of nearly 40 °C was maintained. In addition, the elements were artificially wetted by spraying water onto the end grains of the elements to accelerate the climatization. In the second series, the achieved moisture content for specimen P19 and P21 at the start of the tests was around 18 M%.

5.2.2 Effect of End-grain sealing

The moisture content variations of the elements P2 (open end grain) and P3 (sealed end grain) are directly compared in Figure 34. Following observations regarding P2 and P3 can also be seen for the elements P6 and P7 in Figure 33. In P3, the moisture content measured at the end grain (SH) and in the middle (MI) of the specimen overlap for both depths at 15 mm and 40 mm with different speed. The sealing resulted in an equal moisture content along the complete length of the element. Thus, there is no gradient along the specimen for the sealed ones. No differentiation of the moisture content results at end grain and middle of the specimen must be made.

Once the end grain is not sealed like in P2, the moisture content in the cross section near the end grain reduces more rapidly for both depths with the same speed. For the unsealed specimens, there is not only a moisture gradient over the width of the element, but also along the length. However, this effect is small. Even then moisture content change at end grain is quicker for the first days, they harmonize after about 25 days over the length of the specimen, see Figure 33. Therefore, the influence of the end grain on the behaviour of the reinforcement in the middle of the specimen is neglected and the moisture values taken in the middle (MI) of the specimens are used for the evaluations of the moisture behaviour and the hygro-expansion calculations within chapter 5.6.
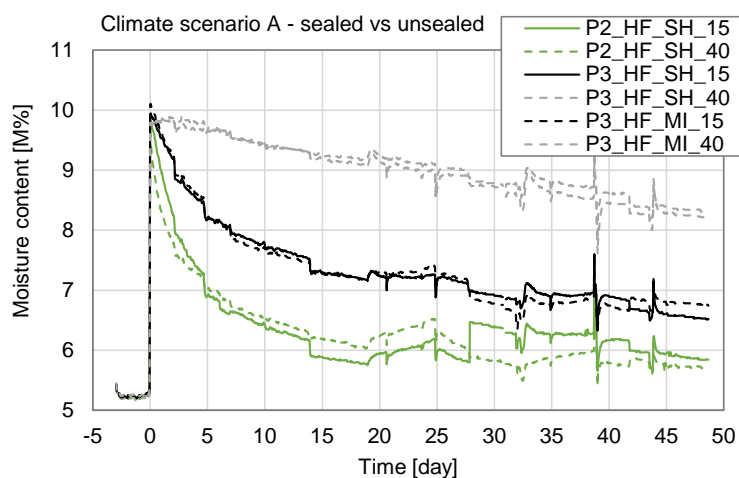
Figure 34: Moisture development in P2 (unsealed) and P3 (end grain sealed)

5.2.3 Calculation of average moisture content over the cross section

To be able to relate all further calculations respectively results per moisture content or moisture content change, an effective moisture content as the average moisture content over the cross section was used. It was calculated using the trapezoid rule according to Eq. (18) and as shown in Figure 35. The moisture content at the surface of the element could not be measured. Instead, the theoretical equilibrium moisture content from the surrounding climate was used. The centre of the width was assumed to have the same moisture content as the 40 mm deep electrode. The tests did not last sufficiently long to expect large differences between the 40 mm deep electrode and the mid-section at 80 mm depth. The procedure is illustrated in Figure 35.

$$\overline{u} = \frac{15 \cdot \left(u_{surf} + u_{15}\right)/2 + 25 \cdot \left(u_{15} + u_{40}\right)/2 + 40 \cdot u_{40}}{80} \tag{46}$$

During wetting of the element, the moisture content is overestimated. During drying, it is underestimated.
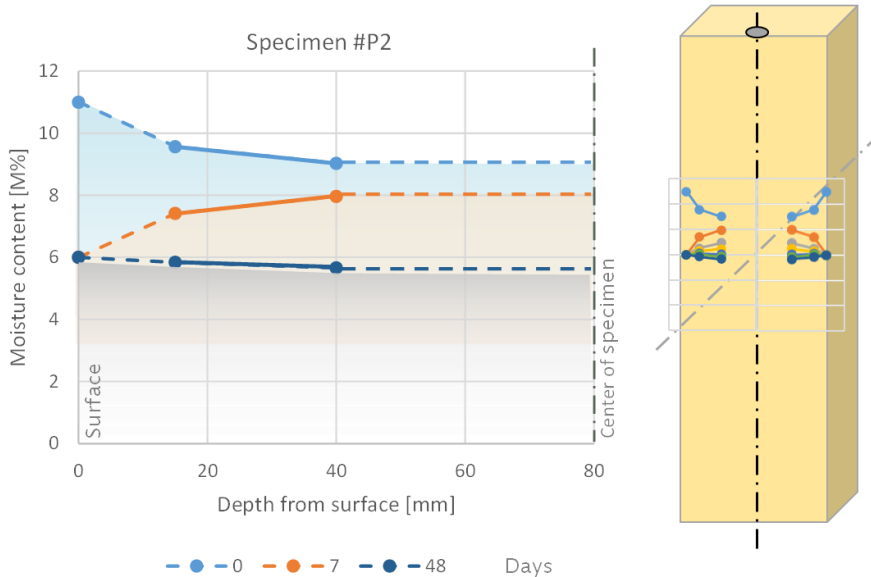
Figure 35: Illustration of the interpretation of the moisture content distribution in the 160 mm wide cross sections where 15 mm and 40 mm long electrodes were used for three separate days. Moisture content is assumed to be constant between 40 mm and 80 mm depth. Moisture content at the surface is according to the equilibrium moisture content of the surrounding climate.

5.2.4 Moisture content

The change of moisture content from the beginning to every individual measuring event was calculated with the averaged moisture contents over the width. Due to the restricted numbers of moisture measurements, thus, not all specimens could be measured and following assumptions are made for the further evaluations:

▸ P2 and P6 are the basis for all unsealed specimens:
  - For the short specimens P1 and P5, the end grain measurements (SH) of their counterparts P2 and P6 have been used: P1 = P2-SH and P5 = P6-SH
  - For the longer specimens P4 and P8, the results are assumed to be equal to that of element P2 and P6: P4 = P2-MI; P8 = P6-MI

▸ P3, P15, P7 (600 mm high) and P13, P17, P21 (1000 mm high) are the basis for all end grain sealed specimens:
  - P23 and P12 = P3 (sealed, 600 mm high, scenario A)
  - P24 and P14 = P13 (sealed, 1000 mm high, scenario A)
  - P25 and P16 = P15 (sealed, 600 mm high, scenario B)
  - P26 and P18 = P17 (sealed, 1000 mm high, scenario B)
  - P27 and P20 = P7 (sealed, 600 mm high, scenario C)
  - P28 and P22 = P21 (sealed, 1000 mm high, scenario C)

The moisture content changes are calculated at the time that deformation measurements were made. The overview is shown in Figure 36. Even though, the specimens start at different moisture levels, the change in moisture content is very similar for the same configurations (sealed/non sealed). In addition, no influence of the specimen height can be seen, cp. P13 with P3, P11; P15 with P17; P21 with P7, P19. The

moisture content change at the end grain is quicker than in the middle of the specimen and reach almost the same values after 40 days for climate scenario A. The sealed specimens decrease in moisture content of about 2.5 M% in climate scenario A and 4 to 6 M% in climate scenario C, whereas the unsealed ones decrease up to 4 M% and 7 M% respectively. In climate scenario B, the moisture content increase by 2 M% within the 35 days of wetting and decreases by 4 M% during the drying phase.
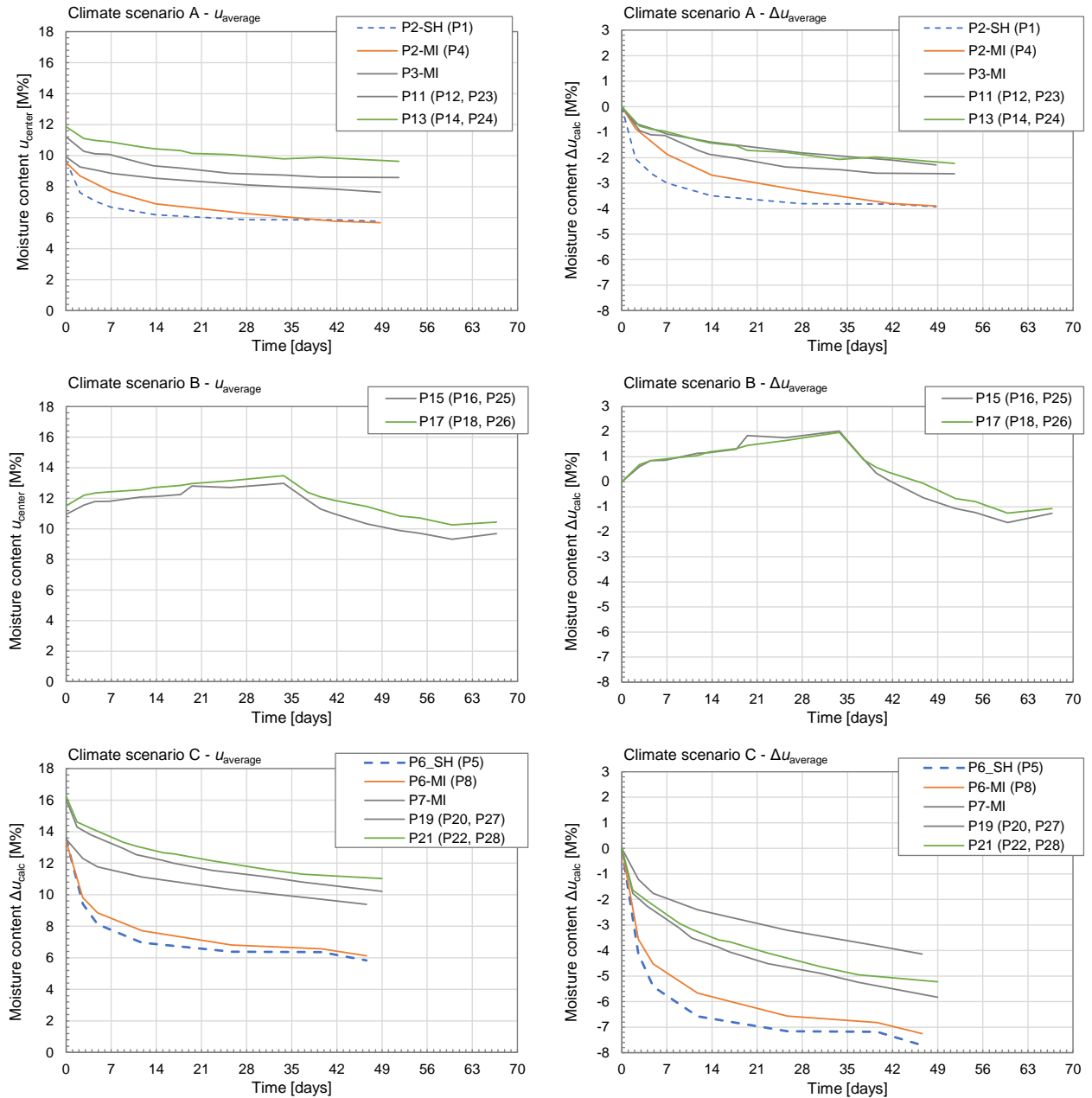
Figure 36: Calculated average moisture contents (left) and changes (right) of the elements

5.3 Deformations

5.3.1 Deformation of the mechanical reinforcement as average strain

The deformations of the screws (relative to their length after insertion as an average strain (eps) are summarized in Figure 37. Right after the start or right after a change of climate, the deformations were measured more often than close to the end of the tests. The graphs were given the names according to the element number and the type of measurement of deformation:

- ▸ Px: specimen name
- ▸ R or GS: measured directly on the screw/reinforcement

The name P3-R represents the measurement of the deformation of the screw/reinforcement in specimen P3.
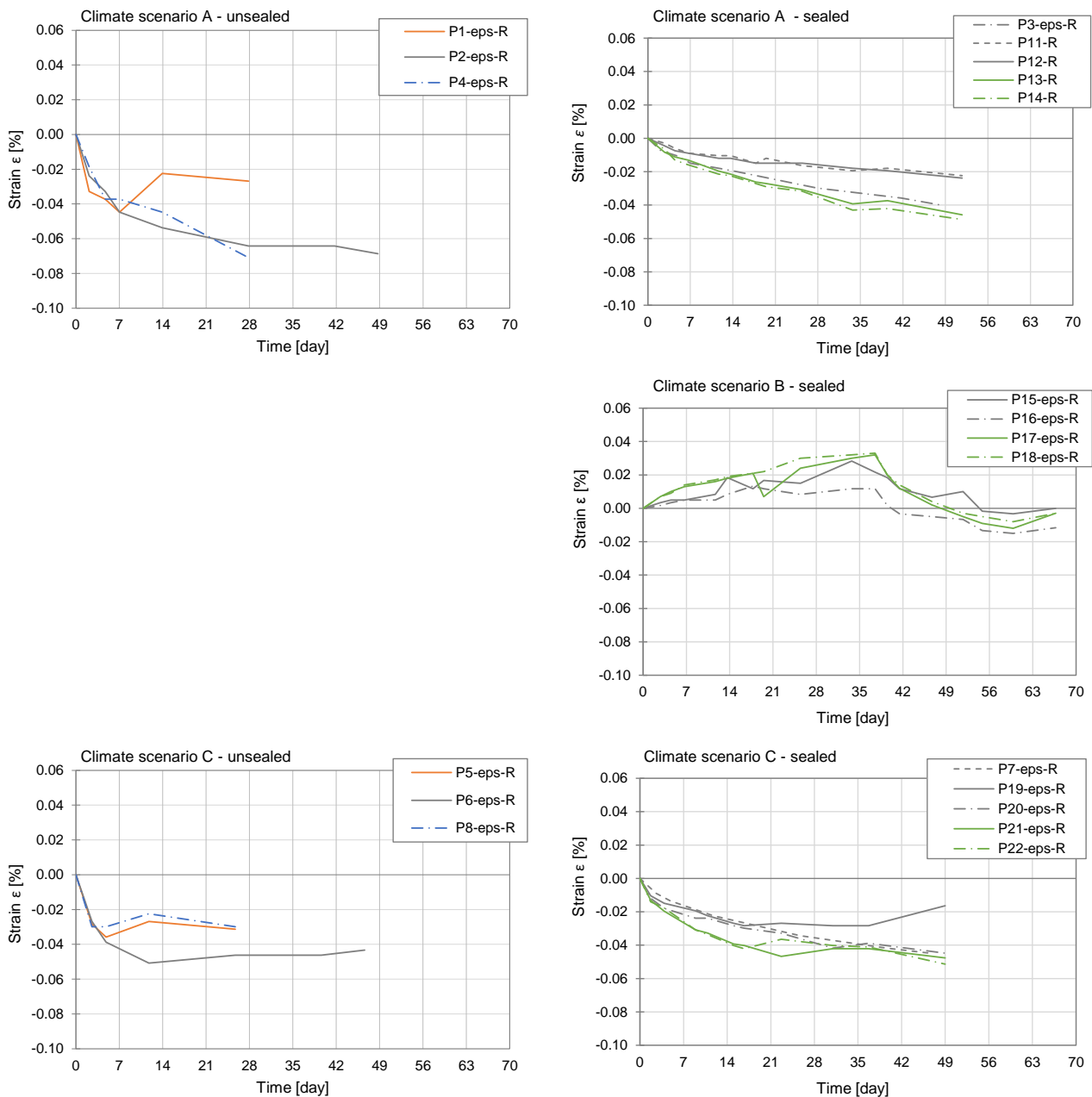
Figure 37: Overview to measured deformations of the screws for all specimens and all three climate scenarios, the unsealed (left) and sealed test specimens (right)

With steadily changing moisture content, the wood deforms and thus also the threaded rod should deform continuously by acting as composite system. This is influenced by cracking of the wood, compare also with crack initiation in chapter 5.5. Following observations are made from Figure 37:

- ▸ The unsealed elements deform more than their sealed counterparts. All deformations for the same configuration are similar.
- ▸ Cracking of the timber surface can be seen in the screw deformations for all unsealed specimens. P1, P4, P5, P6, P8 clearly show an increase or constant value in deformation at a certain day, suggesting the formation of a crack. This is more pronounced for the unsealed specimens. P2 maybe cracks slightly.
- ▸ All sealed specimens in climate scenario A don't show cracking; the length is continuously decreasing.
- ▸ Specimen elements P15 to P18 increase in height initially, but then reduce in height. These elements were first wetted, then dried.
- ▸ Specimen elements of 600 mm height show the tendency to deform slightly less than their 1000 mm counterparts.
- ▸ The specimen in climate scenario C clearly deform quicker at the beginning but also show a tendency for cracking at around 21 days compared to their counterparts of scenario A.

5.3.2   Deformation of the specimen at the wood surface as strain

The deformation of the elements at the surface that were measured are plotted in Figure *38* as strain (eps). A direct comparison between sealed and unsealed as well as scenario A and C are shown in Figure 39. The measurements on side A and side B (left and right side) were averaged. The measurement points were given the names according to the element number, the type of measurement of deformation, and the location:

- ▸ Px: element name
- ▸ eps or DF: deformation results
- ▸ OB, MI, UN: deformation of the three parts across the height OB (top), MI (middle), UN (bottom), as specified in Figure 11
- ▸ W: deformations as sum of OB, MI and UN (larger reference length)

The name Px-eps-MI represents the measurement of the deformation as strain at the surface in the middle part (height-wise) only of element x, whereas Px-eps-W represents the deformations as sum of all single parts of the specimen x.

The following observations from Figure *38* and Figure 39 are made:

- ▸ The deformations of elements P1, P2, P4 of scenario A (small moisture content change) are generally smaller than those of elements P5, P6, P8 of scenario C (larger moisture content change).
- ▸ Both P1 and P5 crack within only 7 days, P6 cracks after 14 days.
- ▸ The stiffness of the reinforcement of element P4 and P8 was twice that of element P2 and P6. All four elements had an unsealed end grain.
- ▸ The end grain sealed elements P3 and P7 deform slower than the unsealed elements P2 and P6.
- ▸ The elements P21 to P22 crack after 20 to 30 days, the element P19 cracks after about 35 days.
- ▸ The average strain on the 600 mm high elements is higher than on the 1000 mm high elements.
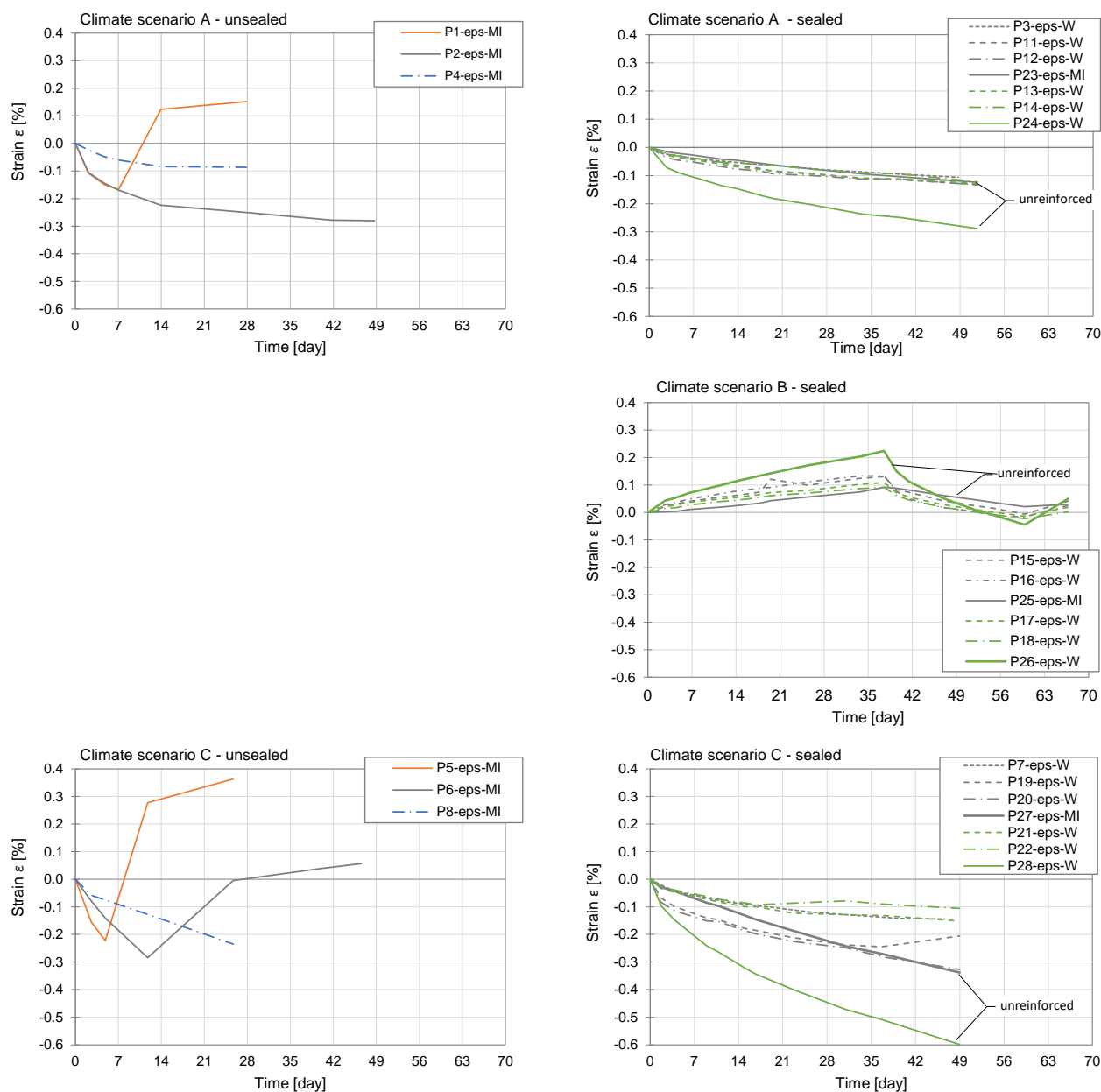
Figure 38: Measured strain for all specimens and all three climate scenarios, the unsealed (left) and sealed test specimens (right)
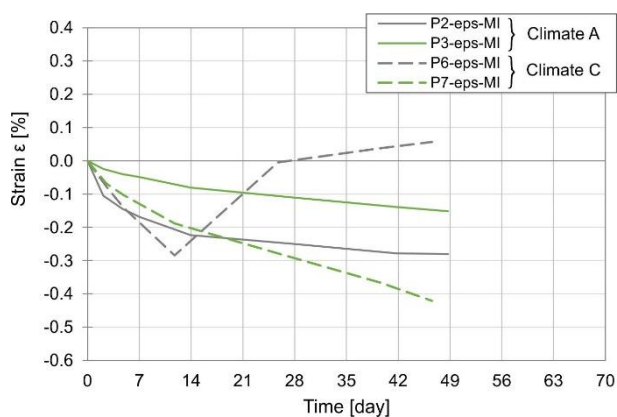
Figure 39: Comparison of measured deformations between sealed and unsealed and climate scenario A and C

5.4 Strain measurements within the reinforcements

Reinforcements of specimens P11, P12, P15, P16, and P19 were instrumented with strain gauges at half length of the screw, as described in 3.3.4.1. The measured strains are plotted in Figure 40. The strains resulting from the global deformations are generally smaller than the ones measured at half length of the rod.

The strain in scenario B in element P15 and P16 increase first, indicating a tensile strain, and the decrease once the elements are dried. After day 60, a swelling is observed again due to a dropout of the climate chamber. The strains on element P19 (scenario C) are larger than on element P11 and P12 (scenario A). On P19 a sudden change is observed indicating crack developments.
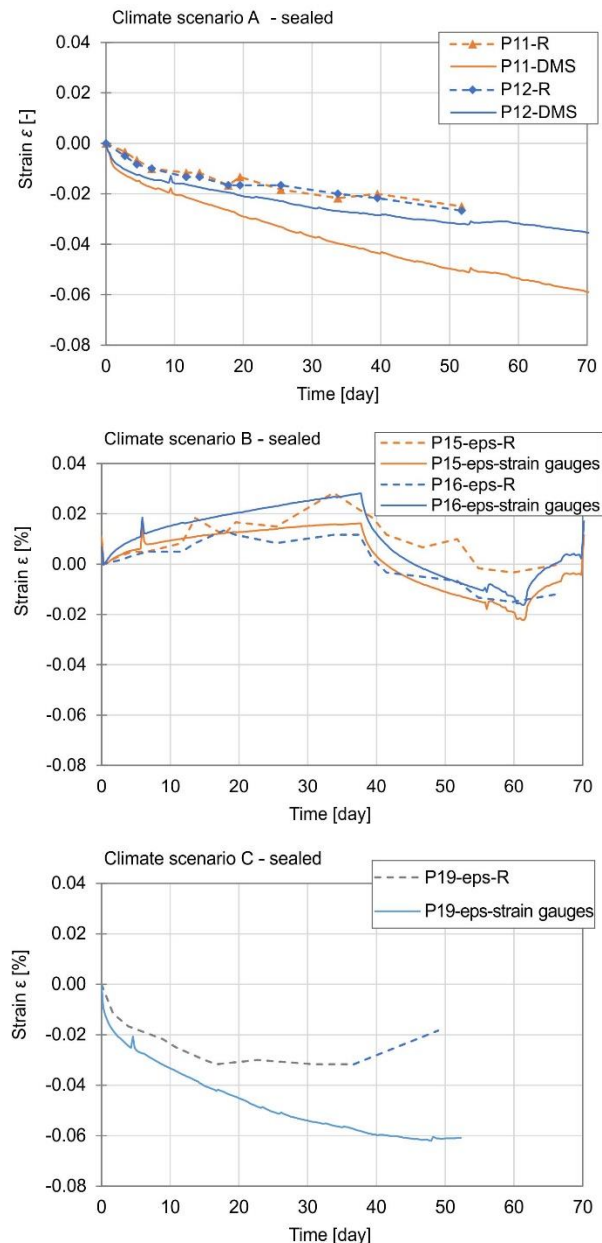
Figure 40: Comparison of the measurement of strains within the reinforcement measured by strain gauges and global deformations at the threated bar (sealed only)

5.5   Failure and observation of cracks

Cracking was recorded for all specimens as e.g., shown in Figure 41 and Figure *42*. In all series the crack growth was marked by drawing a line along the crack and marking the date of identification (optical). For the higher moisture load of about Δ = 12 M% (climate scenario C) more cracks developed at the end grain and even cracks on the side are visible. Almost no cracks are visible at the side for the lower moisture load with Δ = 6 M% (climate scenario A). Specimen with single reinforcement show pronounced larger cracks on one side together with quite large bending deformations compared to the specimen with double reinforcements where the cracks are smaller and more uniformly distributed across the cross section.
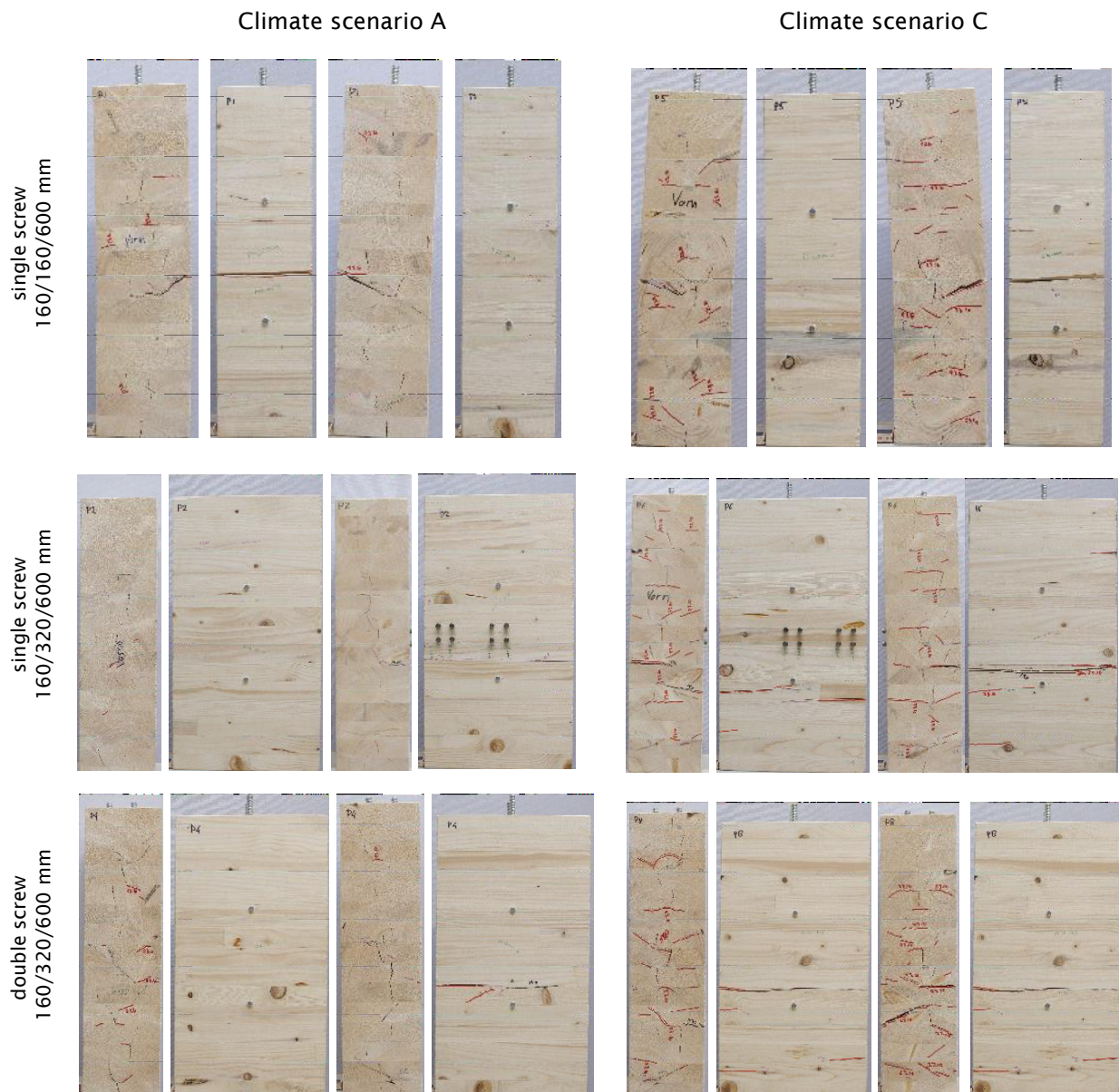
Figure 41: Cracking pattern of the end grain and side view for unsealed specimen P1, P2, P4 of climate scenario A and P5, P6, P8 of climate scenario C

Climate scenario A   Climate scenario C
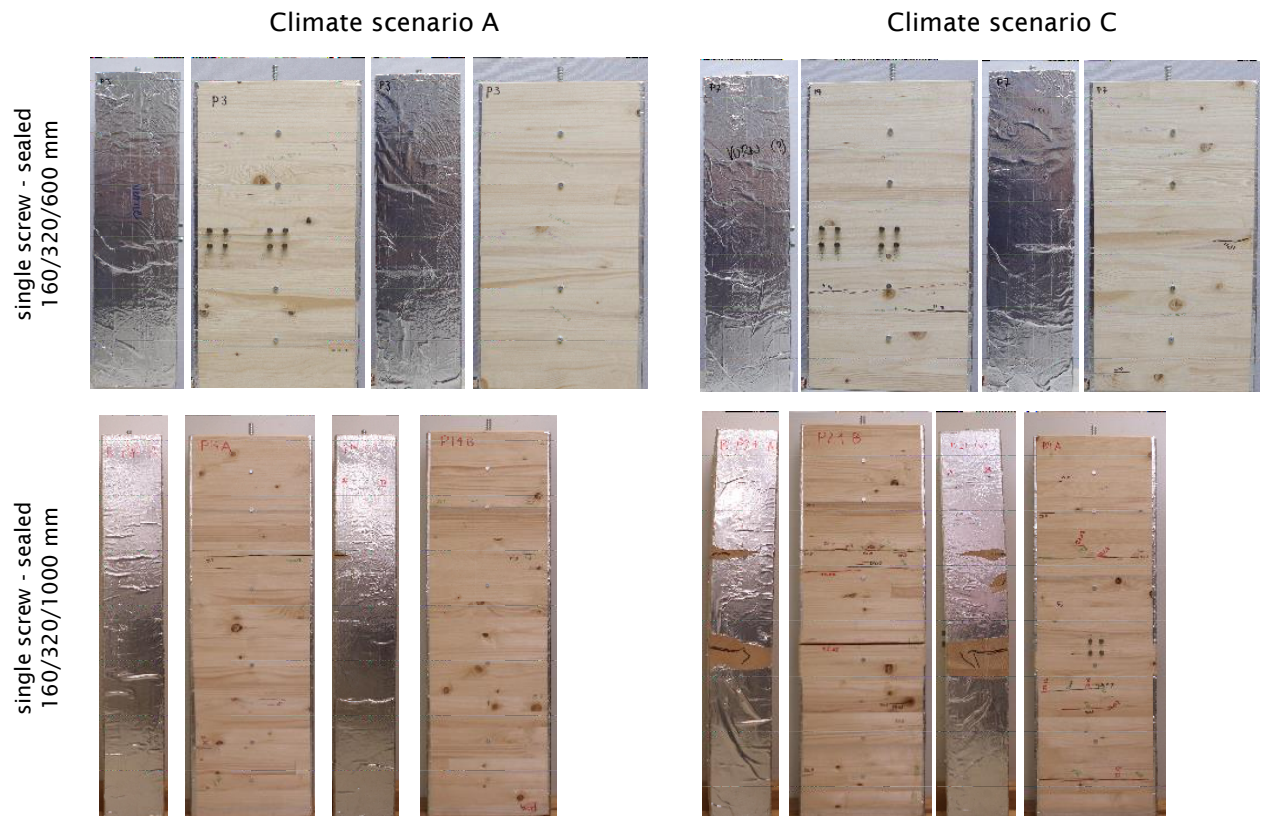
Figure 42: Cracking pattern of the end grain and side view for sealed specimen P3, P13 of climate scenario A and P7, P21 of climate scenario C

The relation between moisture content change and time of cracking is illustrated in Figure 43. The cracked specimens show in average slightly smaller moisture content changes at time of failure compared to the uncracked specimens. P19 was perhaps prone to cracking, as a crack was visible already before the test starts.

- All unsealed elements, except for element P2, cracked
- All sealed elements did not crack, except specimens P21 and P22 both 1000 mm high and with higher moisture change of scenario C
- Elements of scenario C cracked earlier than of scenario A, compare P5 and P8 vs. P1 and P4
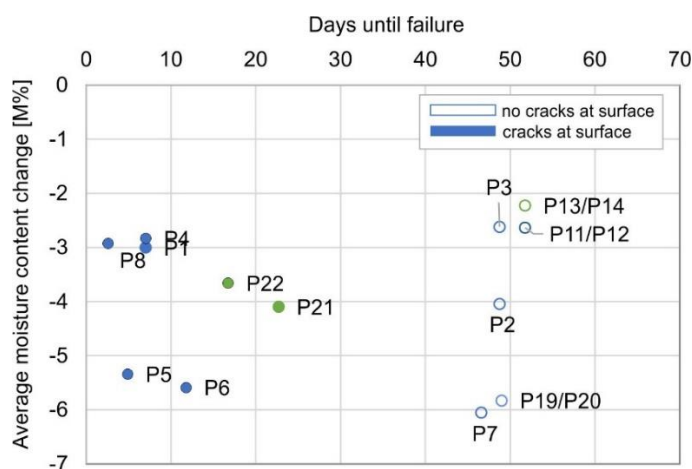
Figure 43: Relation between number of days until failure and related moisture content change for climate scenario A and C

→ It is reasonable to assume that:

- o unsealed specimens crack with small moisture content changes (always end grain cracking → protection required)
- o sealed elements of 600 mm height are unlikely to crack
- o sealed elements of 1000 mm height crack when exposed to higher moisture content changes only

5.6 Characterisation of the hygro-expansion behaviour and factor

5.6.1 Hygro-expansion development

Based on the measured change of moisture content shown before, the dependency of the deformation of the reinforcement on moisture content change can be calculated using the model and equations described in chapter 4 and shown below. This is like an effective hygro-expansion factor, as deformation is calculated as a function of moisture content change. Corrections on height of the specimen is done to obtain the maximum stresses in the reinforcement by the S factor as shown in Figure 28 and towards an infinitely high specimen with factor f as shown in Figure 29. Figure 44 shows the calculated values as a function of time.

$$\gamma = \frac{A_{\text{wood}} E_{\text{wood}}}{A_{\text{wood}} E_{\text{wood}} + A_{\text{steel}} E_{\text{steel}}} \tag{47}$$

$$F_h = \varepsilon_R \cdot S \cdot E_{\text{steel}} \cdot A_{\text{steel}} \tag{48}$$

$$\alpha_{eff} = \frac{\sigma}{\Delta \overline{u} \cdot E_{wood} (\gamma - 1)} = \frac{F_h / f \cdot A_{wood}}{\Delta u \cdot E_{wood} (\gamma - 1)} \tag{49}$$

The following conclusions can be made:

- The hygro-expansion factors stabilise after about 3 days and show a quite constant and consistent development. There is no clear difference between elements with or without end grain sealing. There is, however, a difference in moisture content change, hence, total deformation on unsealed elements will be larger.
- After a change in climatization, elements P15 to P18 display high hygro-expansion factors until stabilizing later. This is due to the small calculation-intervals while having large moisture content changes.
- Higher reinforcement ratios, especially the double reinforced specimens P4 and P8, always show smallest factors compared to their counterparts P2 and P6.

5.6.2 Effective hygro-expansion factor

The calculated hygro-expansion factors can also be plot depending on the final moisture content changes the elements experienced at time of fracture, see Figure 45. Following observations can be drawn:

- No influence of the element height can be seen
- Unsealed elements show larger factors especially at the beginning of the moisture content change and slightly higher factors in average compared to the sealed ones.
- Element P1 shows hygro-expansion factors up to 0.15 %/M%, however time over which these could be derived was very short (only one measurement). It might therefore not be useful.

Generally, the effective hygro-expansion factors are in average 0.06 %/M% which is about 1/4th of the hygro-expansion factor of wood perpendicular to the grain (0.25 %/M%, SIA 265:2021, EN 14080).
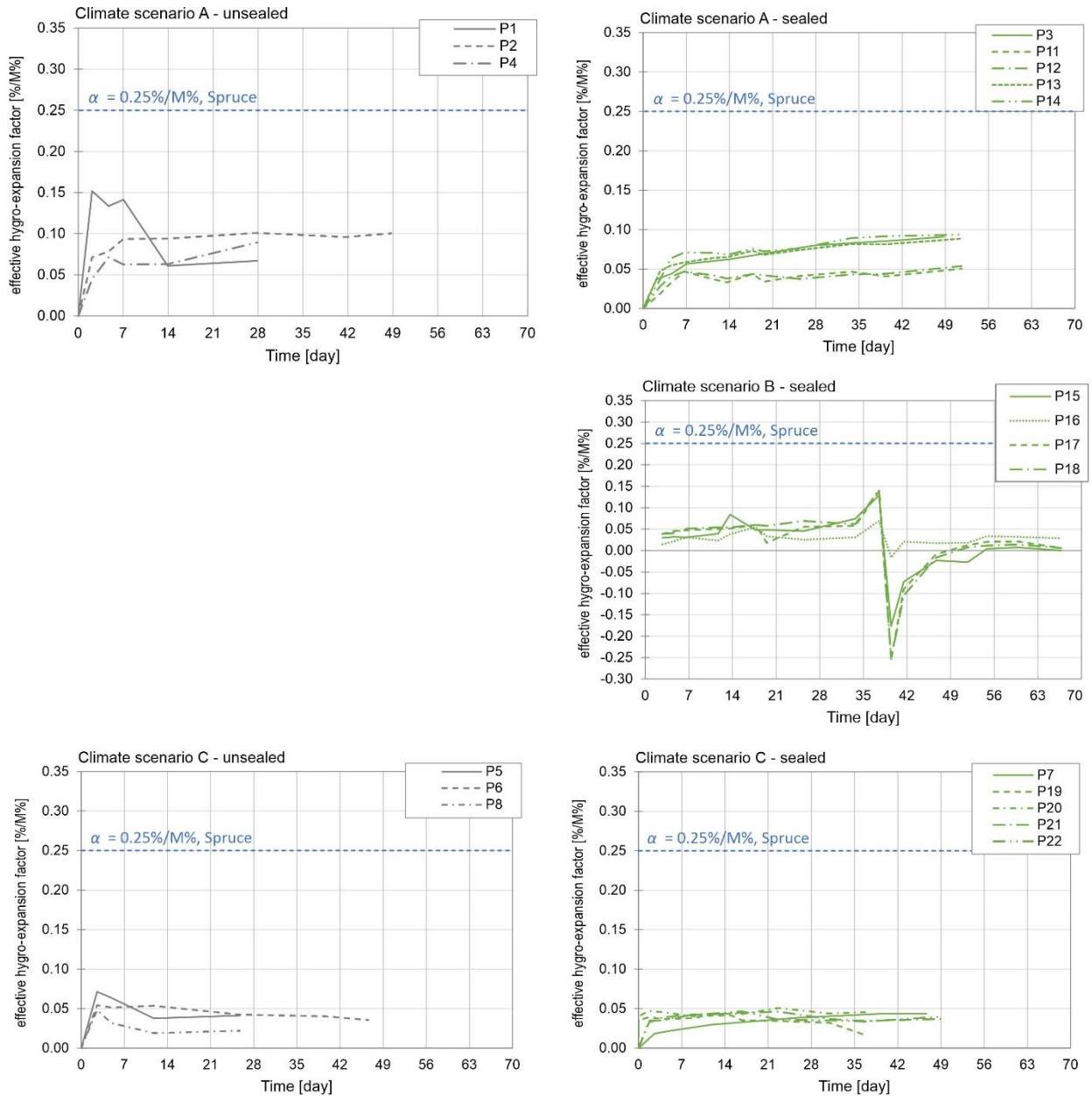
Figure 44: Calculated hygro-expansion factors of the reinforced cross sections
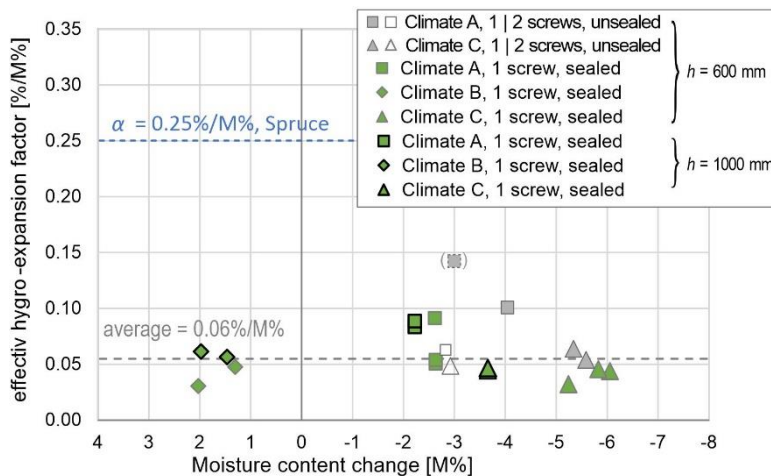
Figure 45: Effective hygro-expansion factors of the reinforced systems in relation to their final moisture content change at time of fracture

5.7 Loads on the screws due to moisture content change

5.7.1 Load development during the moisture impact

By using the model and equations described in chapter 4, the loads on the reinforcements and the timber cross section can be calculated from the measured strains in element 11, 12, 15, 16, and 19, and from the measurement of the total deformations of the reinforcements. The strain on the reinforcements is elastic which means that the strain can simply be multiplied by the modulus of elasticity and the effective cross section to obtain a force. The strain measured with the strain gauges can be used to calculate the total load on the reinforcements. This is done by using the entire cross section of the shaft.

$$F = EA\varepsilon = E_{screw} \frac{D_{screw}^2 \pi}{4} \varepsilon \qquad (50)$$
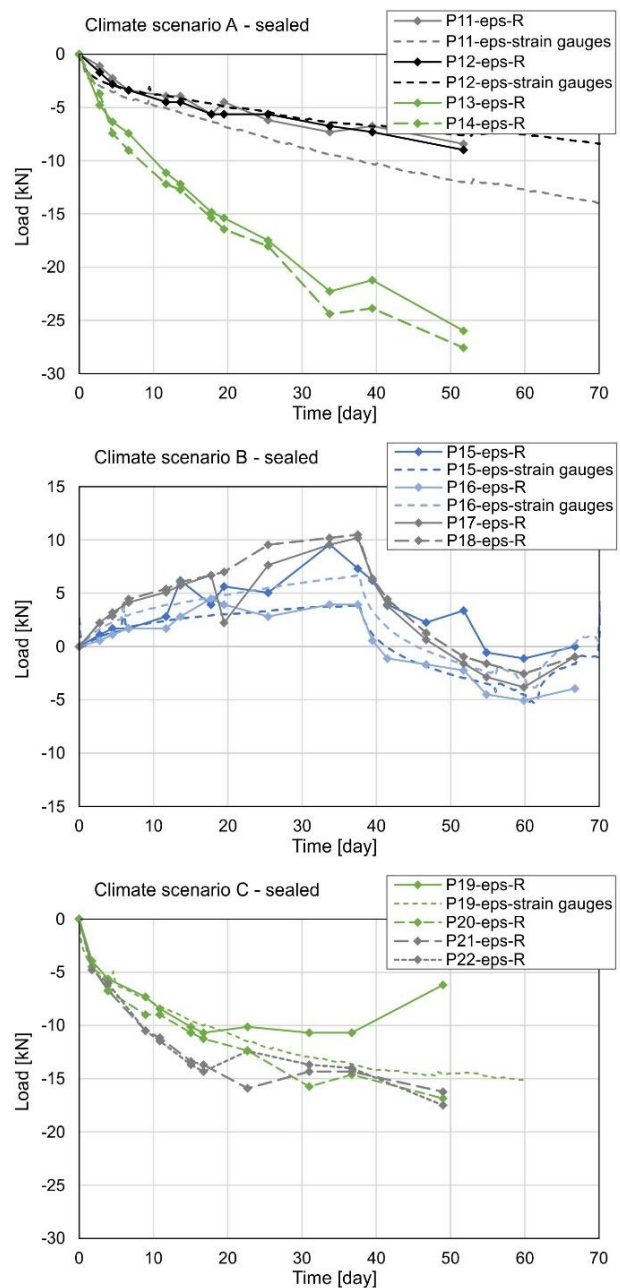
Figure 46: Comparison of the calculated loads from both the strain measurements (Pxx-eps-strain gauges) and deformation measurements (Pxx_eps-R) of the reinforcement

Like the hygro-expansion factor calculations, a correction on height of the specimen is done to obtain the forces in an infinitely high specimen. That is, the loads from the shorter specimens are corrected for by a factor of 0.68, those of the higher ones are corrected for by a factor 0.9. The calculated loads are observed in Figure 46. As observed, the overlap between the two is good.

The tensile loads in P15 and P16 reach levels of 5 kN during wetting, compression loads in P11 and P12 range between 7 to 13 kN. In element P19, loads up to 15 kN were calculated right before failure. What can be observed is, that loads in the reinforcements easily achieve order of magnitudes of 10 kN or even 25 kN. On elements loaded with high moisture content changes, cracks perpendicular to grain occur and the load on the reinforcements reduce or remain at a relative constant level as in climate scenario C.

5.7.2 Calculation of the loads per moisture content change

Using these derived loads, the load per moisture content change at time of fracture can also be calculated. As was seen already in Section 5.6, the hygro-expansion per amount of moisture content change was quite constant. This means that the load on the reinforcement is also quite constant throughout the process of drying or wetting. However, Figure 47 shows that for lower moisture content changes, the values are maybe a bit greater but more divers due to larger fluctuations at the beginning of the moisture impact. For moisture content changes above 3 M% the values are more consistent and below 5 kN/M%. Overall, they show an average value of 5.2 kN/M%, valid for cross section with infinite height.

Figure 47: Loads of the reinforcements per moisture content change at time of failure for infinitely height beams

6 Discussion and recommendations for design

6.1 General information
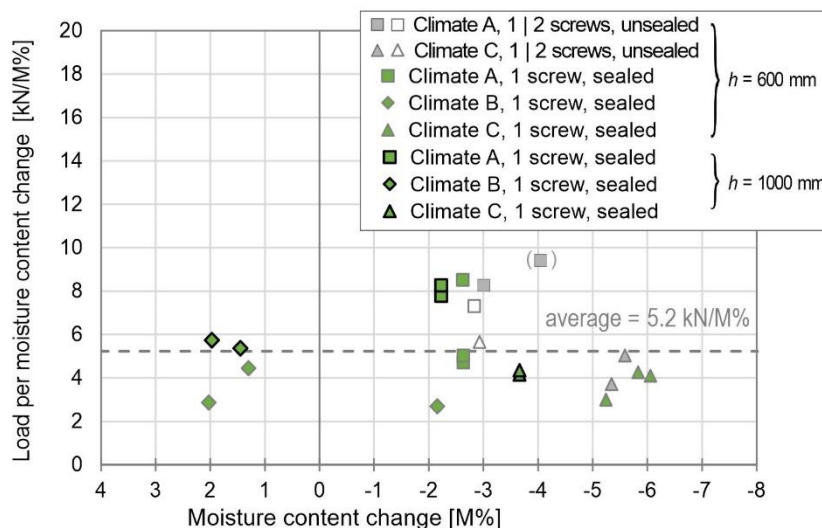
Reinforcements form an important part of timber engineering practice. Whereas theoretically, even small moisture content variations are not allowed because tensile capacity is easily exceeded, reinforced cross-sections experience varying climate without any severe damage. Although moisture content variations on the simplified cross sections showed variations up to several mass percentages, some cross-sections still only showed surface cracks. Cracks in the timber are likely to occur in cases where the cross-section experiences dry climates (drying). The reinforcement acts as a constraint, and it is loaded in compression. Meanwhile the wood experiences tension stresses as it cannot shrink freely.

6.2 Short notes

The following summary can be given to practicing engineers:

- Beams with reinforcements in cross section of 600 mm height are unlikely to develop severe cracking. In high cross sections, the chance that these do occur increases. However, this risk is expected to be equal for cross sections higher than 1.20 m.

- In practice, moisture content variations of a couple mass percentages do not necessarily lead to damaged (severe cracking) cross-sections. This was reflected in the experiments with the 600 mm and 1000 mm high cross sections. The effect of moisture content change combined with loading in tension or shear is not included.

- Sealing end grains of glulam beams, where possible, slows the process of moisture content change throughout the entire cross sections and allows relaxation stresses to develop and reduce the amount of elastic stress on the cross section by around a factor of 2.

- **Reinforcements are best fitted in the factory and not on-site.** Although difficult to execute in practice, the glulam cross section must be produced at a moisture content close to that of its final equilibrium moisture content.

- **Minimum of 2 reinforcements per width of the beam** should be used which severely reduces the risk of large cracks.

- The other possibility is that the reinforcements are implemented once the timber is at its equilibrium moisture content. This is impractical as this can easily take two years and details that need to be reinforced are not accessible anymore. Apart from that, the structural details would be unreinforced in the period until reinforcements are inserted, which is undesirable from a safety point of view.

- To calculate the possible generated additional stress in a cross section due to moisture content changes, the following relation can be used where a **hygro-expansion factor of 0.06 %/M% is recommended**. The γ is the ratio of stiffness between the timber cross section and the total cross-section, a value between 0 and 1:

- $\Delta\sigma_1 = \alpha\Delta u_1 \left(\gamma - 1\right) E_1 \qquad and \qquad \Delta\sigma_2 = \alpha\Delta u_1 \gamma E_2$

- A correction for the depth of the beam can be considered which is almost irrelevant once the depth of the beam is more than 1200 mm high. In low beam depths, it is imagined that the reinforcement is not fully activated as it also needs a certain length to start to react to displacements in the surrounding material.

- Dependencies of the influence of the reinforcement ratio, their spacings, or slenderness on the hygro-expansion behaviour or the load on the reinforcements cannot be characterized with the given results.

6.3   General relation between reinforcement and allowable stress

The developed equations can be used to calculate the maximum moisture content variation when the degree of reinforcement is known. Similarly, the maximum degree of reinforcement can be derived when the expected moisture content variation is known. This will be done using the diagram in Figure 48. The figure shows the stress development as a function of reinforcement EA_2/EA_1 and different moisture content changes.

The following parameters are used: Modulus of Elasticity of 300 N/mm² and a hygro-expansion factor of 0.06 %/M%, an average value that follows from the experiments. If the stiffness of the reinforcement is equal to that of the timber, i.e., EA_2/EA_1 equals 1, a gamma value of about 0.5 is calculated. If the maximum allowable tensile strength perpendicular to the grain for glulam is 0.225 N/mm² (SIA 265:2021) or 0.5 N/mm² (EN 14080), a moisture content variation of about 2.5 M% and almost 6 M% is allowable respectively. The other way around, if a maximum tensile strength of 0.225 N/mm² is allowed and a 4 M% change is expected, the reinforcement can only be 0.5 times higher than that of the wood.

When the depth of the reinforced beam is low, a reduction can be applied as mentioned in Figure 29, i.e., for a 600 mm high beam or effective length of reinforcement, the developed stresses are only 69% of the values listed in idealized case.
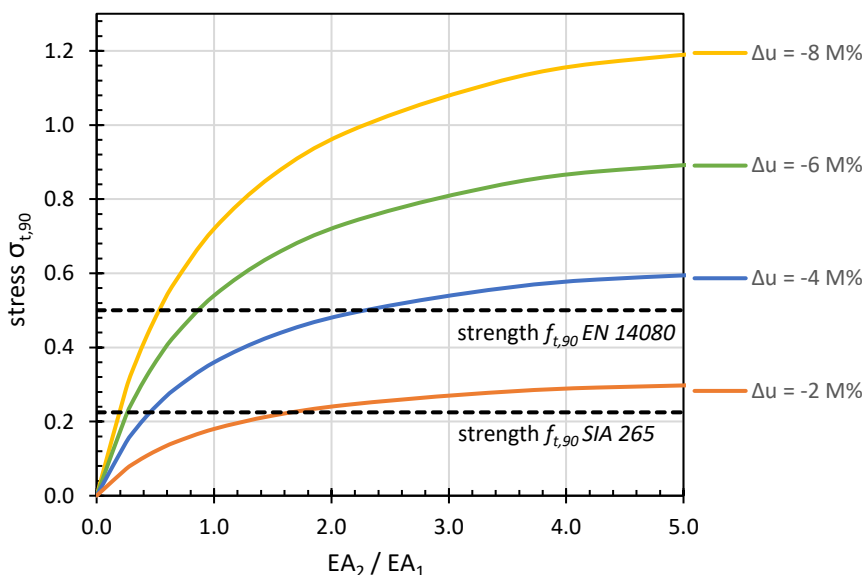
Figure 48: Stress development regarding different moisture content changes and in relation to the reinforcement stiffness ratio

6.4   Load in the reinforcement

The load in the reinforcement is calculated as a function of reinforcement ratio. Figure 49 shows the loads in the reinforcements per percent moisture content change for two different cross section surfaces. No correction for height of the glulam beam is made yet, thus it is valid for an indefinitely high beam, compare chapter 4.2.

It is observed that the larger cross sections generate higher loads on the reinforcement if the stiffness ratio is the same. This is also calculated in the examples in the next section.
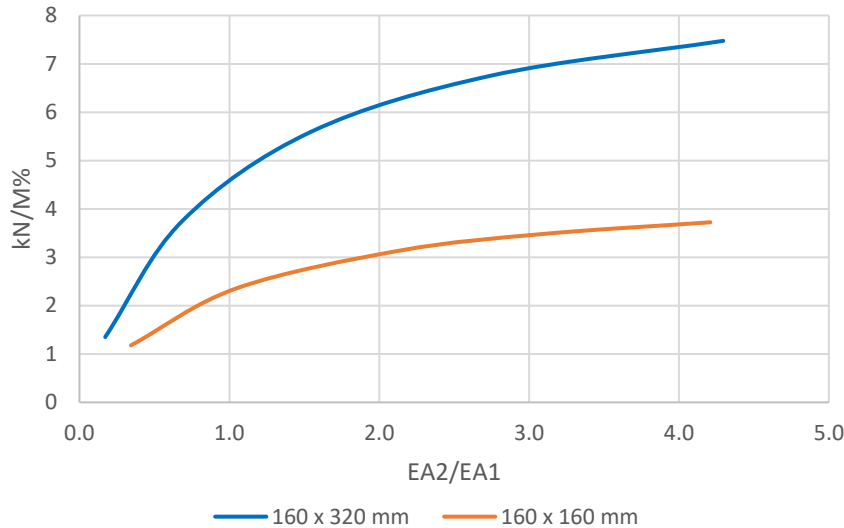
Figure 49: Example of the relation between cross section size and the load in the reinforcement per change moisture content and stiffness ratio

6.5 Design case

There is the case with a cross-section of 240 mm width and 760 mm height. It is a continuous beam, and the reinforcements are be inserted either every a = 250 mm or at a distance of a = 0.75 x h = 570 mm. The diameter of the reinforcement is 16 mm (shaft diameter 12 mm).

In a case where the timber elements are produced at a moisture content of 12 M% and final moisture content is expected around 9 M%, a relatively large degree of reinforcement can be used. If larger moisture content changes are expected, less reinforcement must be applied.

| Material parameter	Reinforcement *a* = 250 mm	Reinforcement *a* = 570 mm
MoE reinforcement, E_2	210'000 N/mm²	210'000 N/mm²
Cross section reinforcement, A_2	12² x π/4 = 113.1 mm²	12² x π/4 = 113.1 mm²
MoE wood, E_1	300 N/mm²	300 N/mm²
Cross section wood, A_1	240 x 250 mm = 60'000 mm²	240 x 570 mm = 136'800 mm²
EA_2/EA_1	1.32	0.58
Reinforcement ratio, γ	0.43	0.63
Maximum allowable stress	0.225 N/mm²	0.225 N/mm²
Maximum allowable moisture content change, Δu	2.2 M%	3.41 M%
Load reinforcement (idealized)	13.5 kN (compression) with $\Delta\sigma_2 = \alpha_1 \Delta u_1 \gamma E_2$	30.8 kN (compression)

The essential equations are listed again:

The ratio of reinforcement can be calculated using: $\gamma = \dfrac{A_1 E_1}{A_1 E_1 + A_2 E_2}$

In idealized cases, the stress in the timber can be calculated using: $\Delta\sigma_1 = \alpha_1 \Delta u_1 (\gamma - 1) E_1$,

and the stress in the steel reinforcement can be calculated using: $\Delta\sigma_2 = \alpha_1 \Delta u_1 \gamma E_2$

In case the beam depth is low, a reduction of the stresses can be applied with factor f, it generally depends on the interaction/stiffness between timber and reinforcement.

7 Conclusions

The discussion with practicing engineers resulted in a focus of the experiments to drying of reinforced cross sections. Two test series were performed of which the first was performed to test the measurement setups. A third test series would have been valuable for sake of statistics. Also, resources should have been reserved to test material parameters in detail, i.e., Modulus of Elasticity of each individual board.

The chosen instrumentation was suited for the planned tests. The obtained measurement values for deformation and moisture content change were good. The availability of climate chambers over long periods of time is a problematic issue. Selected cross sections were not very wide which allowed faster drying of the wood, but still drying over four months instead of only two could have resulted in more fractured cross-sections since stresses in the cross sections could develop over longer periods of time.

The experiments resulted in valuable data and observations:

- The difference in damage between sealed and unsealed end grains was obvious. This was likely due to the high moisture content changes over short periods of time.
- When dividing deformation by moisture content, constant values could be derived. This suggests that over longer periods of time, it is possible to use simplified models to realistically estimate things like deformations, generated stresses, and loads.

Using a simplified numerical model, chapter 4, a height effect was observed that converges once the cross section is higher than 1.2 meters. For smaller cross sections of 600 mm height, it was concluded that only surface cracks occur even close to 6 M%, unless the end grain is unsealed which allows a very rapid moisture content change. On the higher cross sections, moisture content of more than 4 M% lead to a cracked cross section, from one side up to the reinforcement.

Using a second simplified model, chapter 5, effective hygro-expansion factors could be calculated. In these calculations, theoretical design values for E-moduli (300 N/mm^2) had to be used. An important conclusion is that whereas theoretical hygro-expansion values of wood perpendicular to the grain lie around 0.25 %/M% (SIA 265, 2012), these might lie close to a quarter of this value in reality. This explains why larger moisture content values are possible without cracking and reflect reality more. Using a value of 0.06 %/M% in combination with a correction for a height effect, allows estimation of realistic moisture induced strain changes of reinforced glulam cross-sections. The 0.06 %/M% does not reflect the real hygro-expansion coefficient but is expected to be more of an 'effective' value that includes effects of mechano-sorptive relaxation and time-dependent creep too under the presence of reinforcements. To calculate the possible generated additional stress in a cross section due to moisture content changes, Eq. (9) can be used where a hygro-expansion coefficient of 0.06 %/M% is recommended in average.

Also, loads in the reinforcements could be estimated using a moisture content dependent 'hygro-load' factor which was around 5.2 kN/M%. The order of magnitude of loads in the experiments was up to 15 kN in the reinforcements. This could be verified using strain gauges that were glued into the reinforcements. This is considerable, seen that this is about 15% of the capacity of the reinforcements itself. During wetting of a cross section, these loads develop into tension loads. For now, it is likely that these values hold only for the cross sections used in these experiments.

It is clear, that the measurement setups could be used to obtain valuable data that was not present before for these large cross sections. Principles could be used for more tests. Still, combination of combined tensile loading (in notches or holes) and moisture content change was not tested, nor was residual load after climatization tested. That means that the impact of the results is positive and helps to understand the observations made in practice better, but that the applicability to a real recommendation for practice of building standards is limited. Principles can be used to continue investigations.

As a result of the test and the resulting work with the simplified models, the following recommendations are listed:

- A larger variety of cross section areas should be tested in experiments. Different lengths and widths of cross sections can be produced, with different (arrangement of) reinforcements.
- The results indicate that there is a significantly lower hygro-expansion ratio in practice than in theory. This should be tested for different reinforcement ratios and cross section surfaces.
- Further investigation of the effect of beam height on the loads in the reinforcement.
- To better understand what and how the stresses and loads develop throughout the glulam beam, 3D simulations should be performed. Some experimental studies exist, but it is still difficult to quantify an 'activated volume', i.e., the volume experiencing constrained stress. Studies like presented by Danzer and Dietsch (2020) show that there is effect of height as was seen here the height effect and that there is an effect of stiffness ratio.
- For a complete validation with the data from the experiments, Moduli of elasticity and hygro-expansion factors of each board should be measured and inserted into a 3D-FE simulation separately.

8 Bibliography

Aicher S., Dill-Langer G. (1997), Climate induced stresses perpendicular to the grain in glulam, Otto-Graf Journal 8, pp. 209-231

Angst V., Malo K.A. (2013) Moisture-induced stresses in glulam cross sections during wetting exposures, Wood science and technology 47, 227-241

Angst V., Malo K.A. (2012), Effect of self-tapping screws on moisture induced stresses in glulam, Engineering Structures, Vol. 45, pp. 299–306

Angst-Nicollier V. (2012), Moisture induced stresses in glulam - effect of cross section geometry and screw reinforcement, PhD thesis 2012:139, NTNU Trondheim, Norway

Birschke C., Rapp A., Bayerbach R., Morsing N., Fynholm P., Welzbacher C. (2008) Monitoring the ''material climate'' of wood to predict the potential for decay: Results from in situ measurements on buildings, Building and Environment 43, pp. 1575–1582

Blaß H. J., Bejtka I., Uibel T. (2006), Tragfähigkeit von Verbindungen mit selbstbohrenden Holzschrauben mit Vollgewinde, Universitätsverlag Karlsruhe, Karlsruhe

Blaß H. J., Krüger O. (2010), Schubverstärkung von Holz mit Holzschrauben und Gewindestangen, Karlsruher Berichte zum Ingenieurholzbau, Band 15, Karlsruhe

Blaß H. J., Ehlbeck J., Kreuzinger H., Steck G. (2004) Erläuterungen zu DIN 1052:2004-08 Entwurf, Berechnung und Bemessung von Holzbauwerken, DGfH Innovations und Service GMBH München

Blaß H. J. (2017), Selbstbohrende Schrauben und Systemverbinder - Stand der Technik und Herausforderungen, 23. Internationales Holzbau-Forum, Garmisch-Partenkirchen

Danielsson H. (2013), Perpendicular to grain fracture analysis of wooded structural elements - models and applications, Doctoral Thesis, Lund University, Sweden, ISBN: 978-91-7473-475-1

Danzer M., Dietsch P., Winter S. (2020) Shrinkage behaviour of reinforced glulam members, INTER International Network on Timber Engineering Research, online meeting, Karlsruhe 2020

Danzer M., Dietsch P., Winter S. (2022) Effect of shrinkage on cracking and structural behaviour of reinforced glulam members, Construction and Building Materials, Volume 327, 1-14

Dietsch P. (2012), Einsatz und Berechnung von Schubverstärkungen für Brettschichtholzbauteile, Dissertation, Technische Universität München

Dietsch P., Brandner R. (2015), Reinforcement with self-tapping screws and threaded rods in Reinforcement of timber structures: a state-of-the-art report, Construction and Building Materials 97, pp. 78–89

Dietsch P., Franke S., Franke B., Gamper A., Winter S. (2015) Methods to determine wood moisture content and their applicability in monitoring concepts, Journal of Civil Structural Health Monitoring 5, 115–127

Dietsch P. (2017) Effect of reinforcement on shrinkage stresses in timber members, Construction and Building Materials 150, pp. 903-915

Dietsch P, Winter, S. (2018) Structural failure in large-span timber structures: A comprehensive analysis of 230 cases. *Journal of Structural Safety*, 71, 41-46.

Dyken T. and Kepp H. (2010) Monitoring the Moisture Content of Timber Bridges, presented at the ICTB, International Conference on Timber Bridges, Lillehammer, Norway

Ehlbeck J., Belchior-Gaspard P., Gerold M. (1992), Eingeleimte Gewindestangen unter Axialbelastung bei Übertragung von großen Kräften und bei Aufnahme von Querzugkräften in Biegeträgern, Forschungsbericht, Universität Karlsruhe, Karlsruhe

Forsén H. and Tarvainen V. (2000) Accuracy and functionality of hand-held wood moisture content meters, Technical Research Centre of Finland, VTT Publications 420, Espoo, Finland

Franke B., Franke S., Müller A. (2014) Case studies: long-term monitoring of timber bridges, Journal of Civil Structural Health Monitoring 5 (2), pp. 195-202

Franke B. and Quenneville P. (2011) Numerical Modeling of the Failure Behavior of Dowel Connections in Wood, Journal of Engineering Mechanics 137(3), pp.186-195

Franke B., Müller A., Franke S., Magnière N. (2016), Langzeituntersuchung zu den Auswirkungen wechselnder Feuchtegradienten in blockverleimten Brettschichtholzträgern, Research Report Berner Fachhochschule, ISBN 978-3-9523787-7-9

Franke B. (2017), Holzfeuchte smart kalkuliert für moderne Tragquerschnitte, S-Win Kurs 2017, Weinfelden, Schweiz

Franke S., Franke B. Harte A.M. (2015), Failure Modes and reinforcement techniques for timber beams – State of the Art, Construction and Building Materials 97 (2015) 2–13

Franke S., Franke B., Magnière N., Steiger R., Jockwer R. (2016), Assessment of the residual load-carrying capacity of large span members in wood, Forschungsbericht, ISBN 978-3-9523787-9-3

Franke B., Schiere M., Franke S. (2018), Stress developments in large timber cross sections in relation to the climate and strength class, WCTE 2018, South Korea

Frese M., Blass H.J. (2011) Statistics of damages to timber structures in Germany, Engineering Structures, 33 (11), 2969–2977

Gamper A., Dietsch P., Merk M. (2012) Gebäudeklima – Langzeitmessung zur Bestimmung der Auswirkungen auf Feuchtegradienten in Holzbauteilen, Research Report, Technical University of Munich, Germany, ISBN 978-3-8167-9518-6

Gamper A., Dietsch P. (2015), Gebäudeklima - Langzeitmessung zur Bestimmung der Auswirkungen auf Feuchtegradienten in Holzbauteilen, Research Report, Technical University of Munich, Germany, Fraunhofer IRB Verlag 2015, ISBN 978-3-8167-9518-6

Gerold M. (1992), Verbund von Holz und Gewindestangen aus Stahl, Bautechnik (69), Heft 4

Gustafsson PJ., Hoffmeyer P., Valentin G. (1998), DOL behaviour of end-notched beams, Holz als Roh- und Werkstoff 56, 307-317

Hedlin C.P. (1968) Sorption Isotherms of twelve species at subfreezing temperatures, Forest Products Journal, Vol. 17, p. 43-48

Hansen K. (1986) Sorption isotherms – A catalogue, Technical University of Denmark, De-partment of Civil Engineering, Building Materials Laboratory, Technical Report162/86

Jockwer R. (2014), Structural behavior of glued laminated timber beams with unreinforced and reinforced notches, Dissertation No. 21825, ETH-Zurich, Switzerland

Koj C., Trautz, M. (2014), Mit Schrauben fügen und bewehren – Langzeitversuche an biegesteifen Rahmenecken im Aussenklima, Bautechnik 91 (2014), Heft 1

Lauber B. (2008), Ertüchtigung von Holztragwerken, Beispiele aus der Praxis, Holzbautag 2008, Biel/Bienne, Schweiz

Melin C., Gebäck T., Heintz A., Bjurman J. (2016) Monitoring dynamic moisture gradients in wood us-ing inserted relative humidity and temperature sensors, e-Preservation Science, 1581-9280 (eISSN), Vol. 13, p. 7-14

Norsk Treteknisk Institut (2013) Monitoring five timber bridges in Norway - results 2012, Report no. 310332, Oslo, Norway

Schiere M. (2016) Moisture diffusion and moisture induced stresses in glulam cross-sections, MSc Thesis, BFH Bern, Switzerland, thesis no. MHT/PA/MA/045/16/00

Schiere M. (2018), Moisture content of Timber Structures in Varying Ambient Climates, STSM report, COST Action FP1402

Schiere M, Franke S, Franke B (2020), Quality assurance and design of timber structures in varying climates, Inter Conference proceedings, Karlsruhe, 2020

SIA 265 (2012) Holzbau, Schweizerischer Ingenieur- und Architektenverein, Zurich, Switzerland

SIA 265/1 (2018) Holzbau - Ergänzende Festlegungen, Schweizerischer Ingenieur- und Architektenverein, Zurich, Switzerland

Sjödin J. (2008) Strength and moisture aspects of steel timber dowel joints in glulam structures - an Experimental and Numerical Study, Thesis (PhD). Växjö University.

SN EN 1995-1-1 (2004), Eurocode 5: Bemessung und Konstruktion von Holzbauten – Teil 1-1: Allgemeines, Schweizerischer Ingenieur und Architektenverein, Zürich

SN EN 14080 (2013), Holzbauwerke - Brettschichtholz und Balkenschichtholz – Anforderungen, Schweizerischer Ingenieur- und Architektenverein, Zurich, Switzerland

Steiger R., Serrano E., Stepinac M., Rajcic V., O'Neill C., McPolin D., Widmann R. (2015), Strengthening of timber structures with glued-in rods, Construction and Building Materials 97, pp. 90–105

Trautz, M. (2017), Das Dehnungs- und Tragverhalten von Brettschichtholz beim Lasteintrag durch Vollgewindeschrauben, Bautechnik 94, Heft 11

Trautz, M. Koj, C. (2008), Mit Schrauben bewehren, Bautechnik 85, Heft 3

Volkersen, O. (1938), Die Nietkraftverteilung in zugbeanspruchten Nietverbindungen mit konstanten Laschenquerschnitten, Luftfahrtforschung Band XV, Verlag Oldenbourg, Berlin Aldersdorf

Wallner B. (2012), Versuchstechnische Evaluierung feuchteinduzierter Kräfte in Brettschichtholz verursacht durch das Einbringen von Schraubstangen, Master Thesis, TU Graz, Graz, Austria.